A Novel Approach to the Part Orientation Problem for Robotic Assembly Applications

Brian James Slaboch
Marquette University

A NOVEL APPROACH TO THE PART ORIENTATION PROBLEM FOR ROBOTIC ASSEMBLY APPLICATIONS

by

Brian J. Slaboch, B.S.

A Thesis Submitted to the Faculty of the Graduate School,
Marquette University,
in Partial Fulfillment of the Requirements for
the Degree of Master of Science

Milwaukee, Wisconsin

May 2011

ABSTRACT

A NOVEL APPROACH TO THE PART ORIENTATION PROBLEM FOR ROBOTIC ASSEMBLY APPLICATIONS

Brian J. Slaboch, B.S.

Marquette University, 2011

SCARA (Selective Compliant Assembly Robot Arm) type robots are the most common type of assembly robots. These robots have four degrees of freedom (three rotational and one translational). Typically these robots are used for assembly tasks that take place along a vertical axis. Many times, however, assembly tasks take place along a non-vertical axis.

To account for non-vertical axis assembly, parts must be fed in a proper orientation to allow for correct assembly. Parts feeders and specialized end-effectors are typically used to feed parts in their proper orientation. This thesis investigates a novel end-effector that can be used to feed parts for industrial assembly applications. Specifically, the purpose of the novel end-effector is to provide a SCARA robot with an added selectable degree of freedom.

This end-effector aims to bridge the gap between complex anthropomorphic grippers and simple binary grippers. The approach is novel in that the end-effector interacts with the environment to produce the added degree of freedom. New path planning algorithms were developed to work in conjunction with the novel end-effector. A prototype end-effector was designed, built, and tested to prove the validity of this new approach.

ACKNOWLEDGEMENTS

Brian J. Slaboch, B.S.

I would first and foremost like to thank Dr. Philip A. Voglewede for providing me with this great opportunity. This work could not have been completed without his support and guidance. In addition, I would like to thank Dr. Mark Nagurka and Dr. Joseph Schimmels for their insightful comments and suggestions. A special thanks goes to Jinming Sun and Bryan Bergelin for their continued support and helpful advice. I would also like to thank Tom Silman and Ray Hamilton for their work in the machine shop. Finally, the I would like to thank my family and friends for their encouragement and guidance.

DEDICATION

Brian J. Slaboch, B.S.

I would like to dedicate this work to my family and friends. Without their love and support none of this would have been possible.

Thank You.

TABLE OF CONTENTS

TABLE OF CONTENTS — *Continued*

LIST OF TABLES

LIST OF FIGURES

LIST OF FIGURES — *Continued*

CHAPTER 1

Introduction

Assembly lines were first made famous by Ford Motor Company at the start of the twentieth century. Mass production of automobiles revolutionized manufacturing processes. Businesses realized that a low unit cost per manufactured part led to a competitive advantage. Companies continue to find innovative manufacturing processes that allow them to lower costs and increase quality.

The assembly lines created by Ford have changed significantly from the early 1900's. In many cases, robotic manipulators have replaced human workers on assembly lines. In the automobile industry robots are used for spot welding and other assembly tasks. Robotic manipulators can be used to decrease assembly time and reduce human error. However, one drawback of robotic manipulators is that they lack flexibility. Parts must be fed in a specific part orientation prior to assembly. Current parts feeding devices can lead to high capital costs and offer little flexibility. There is a need to create more efficient and flexible ways to feed industrial parts.

The ability to orient a part prior to an industrial assembly task is known as the part orientation problem. This can include orienting a part prior to grasping it, or this can refer to simultaneous grasping and orientation. As will be shown in this chapter, there are two common approaches to the part orientation problem. These two areas can be broadly categorized into parts feeding systems and end-effector designs (Fig. 1.1). End-effector designs can further be broadly categorized as either complex anthropomorphic hands or simple binary grippers. Complex anthropomorphic hands provide the desired flexibility for industrial assembly tasks but are difficult to control due to the coordination of all of the degrees of freedom (DOF) of the system. Conversely, binary grippers are easy to control but do not provide the necessary flexibility.

This research aims to bridge the gap between the two and determine a way

to combine the flexibility gained from using anthropomorphic hands with the simplicity of binary grippers. To limit the scope of the design problem, this research will focus on end-effector designs that can be used in conjunction with a SCARA (Selective Compliant Assembly Robot Arm) type robot. This research aims to create an end-effector that provides an added DOF to a SCARA robot without adding significant complexity. SCARA type robots were chosen because these are the most commonly used industrial assembly robots [5].

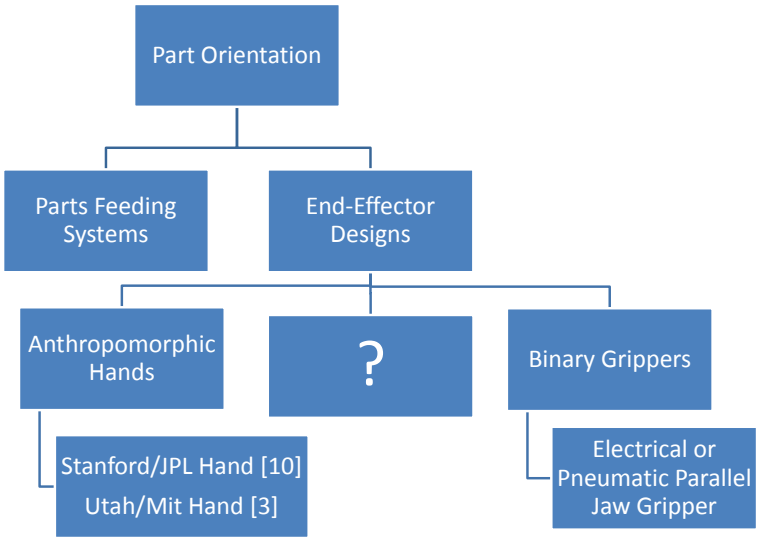

Figure 1.1: Manipulation Flow Chart: The part orientation problem can be broadly categorized into parts feeding systems and end-effector designs.

Four DOF SCARA type robots (three rotational and one translational, Fig. 1.2) are used in many industrial robotic assembly applications. The SCARA robot shown in Fig. 1.2 allows for translational motion as well as a rotation about the z-axis.[1] SCARA type robots work well for assembly tasks and pick and place operations that take place along a vertical axis (i.e., the direction of the gravitational force). This is the most common type of assembly operation. Pick and place assembly tasks are preferred because the parts feeding operation is greatly simplified.

An example of vertical axis assembly is shown in Fig. 1.3. The lever shown in Fig. 1.3a must be picked up, rotated, and then assembled onto the vertical post in

[1]Specifically, this type of motion is known as Schöenflies motion.

Fig. 1.3b. In its natural resting position (Fig. 1.3a), the lever cannot be assembled onto the vertical post using only the DOF of the SCARA robot. The part must be rotated prior to assembly on the vertical post.

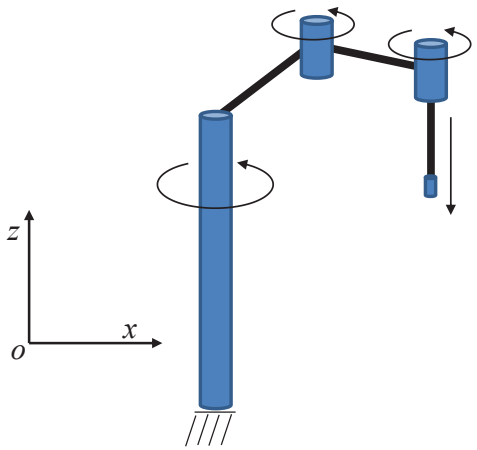

Figure 1.2: SCARA Robot

There are also many robotic assembly tasks and pick and place operations in which a part must be assembled on an axis other than the vertical axis. For instance, consider the six-axis Adept robot shown in Fig 1.4[2] The six-axis Adept robot is able to pick a part oriented along the vertical axis, and it is able to place it on an angled board. This type of angled assembly operation is not possible using only the four DOF of a SCARA robot. The part must be rotated prior to placing it on the angled board.

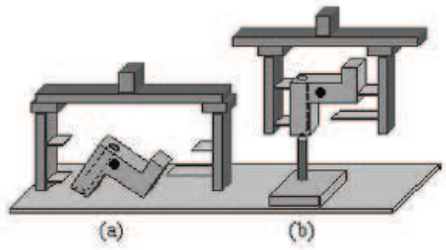

Figure 1.3: Lever Assembly onto Vertical Post [1]

The previous two examples show that proper part orientation is critical for industrial assembly tasks. This chapter reviews previously developed solutions to

[2]Figure 1.4 is used with permission from Adept Technologies Inc.

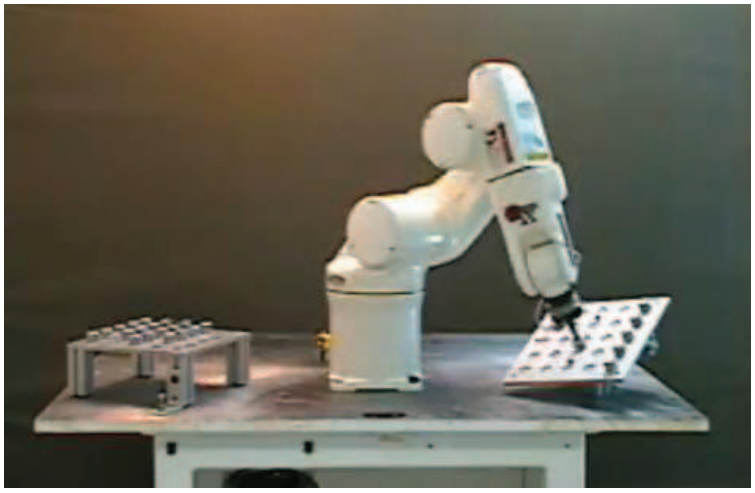

Figure 1.4: Angled Peg Assembly using Adept Viper Robot

the part orientation problem.

1.1 Parts Feeding Systems

The most common approach to the part orientation problem is to use a parts feeding system. Parts feeding systems are typically costly for flexible assembly because they are usually designed for one specific part, and therefore any part change adds significant cost. There are applications in which parts feeders are advantageous. For instance, parts feeders work well for small parts such as screws that have to be stood upright prior to assembly. However, in many situations capital costs can be reduced significantly if vibratory bowl feeders can be eliminated. According to Boothroyd [6], parts feeders are responsible for 30% of the cost and 50% of the failures in assembly operations.

Peshkin and Sanderson [7] developed a parts feeding system that uses a conveyor belt with rigid fences to orient parts prior to assembly. They developed a complete algorithm that can be used to orient polyhedral parts prior to assembly. One drawback from this solution is that the algorithm only works for polyhedral parts. Additionally, the algorithm may not be able to find a solution.

A similar approach to that of Peshkin and Sanderson was completed by Zhang et al. [8] in which parts are fed on a conveyor belt and toppled over by pins. This type of sensorless orientation has the same drawbacks as those of Peshkin and

Sanderson. Another conveyor belt design was completed by Causey and Quinn [9]. Causey and Quinn created a conveyor belt design in which three conveyors work together. This system works for a variety of parts, but it still requires three external conveyors and a separate control algorithm for each part that is fed.

The main drawback with any parts feeding system is that it typically lacks flexibility. The capital costs are typically high, and the parts feeding system must be adjusted for each part. In an attempt to simplify this process, many researchers have focused on parts feeding by grasping and manipulation.

1.2 End-Effector Design

Developing end-effectors that feed parts by grasping and manipulation allows for a more flexible system. Many early end-effector designs mimic the human hand. Examples of these are the Stanford/JPL hand [10], the Utah/MIT Hand [2] (Fig. 1.5), and the Barrett Hand [11]. While these end-effectors are extremely flexible, they are difficult to use in an industrial setting due to the required computational power and coordination of the DOF.

Figure 1.5: Utah/MIT Hand [2]

There have also been attempts at creating industrially feasible end-effectors to orient parts. Goldberg et al. produced a pivoting gripper [3] that uses ball bearings to rotate a part under the force of gravity. They subsequently proved that the pivoting gripper could be used to orient a part arbitrarily in six DOF using a

four DOF SCARA type robot [4]. This gripper uses a series of pivot grasps as shown in Fig. 1.6. In this design, a part is grasped between two ball bearings and rotated under the force of gravity. By completing a series of these pivot grasps the part can be manipulated. The major drawback with this system is that picking up a part repeatedly takes too much time when compared to picking up a part and assembling it directly.

Ziesmer and Voglewede improved upon this design by creating a metamorphic [12] gripper that uses metamorphic joints that change between fixed joints and spherical joints [13]. This reduces the amount of time to manipulate the part. This design is limited in that the part to be picked up must have symmetrical contact points. Ziesmer and Voglewede's design is unique in that they used an external fixed post to pivot the part to a desired angle. One drawback from this design is that it does not work for delicate parts that cannot be pressed into an external fixed finger. Additionally, the ability to use this gripper depends heavily on the part geometry.

In 2002 Zhang et al. showed that it is possible to orient parts while grasping them [8]. Their device is shown in Fig. 1.3. The gripper contact points are used to manipulate the part prior to vertical axis assembly. Once again, this approach only works for polyhedral parts. Furthermore, the approach lacks flexibility because the pin design must be generated for each part to be manipulated.

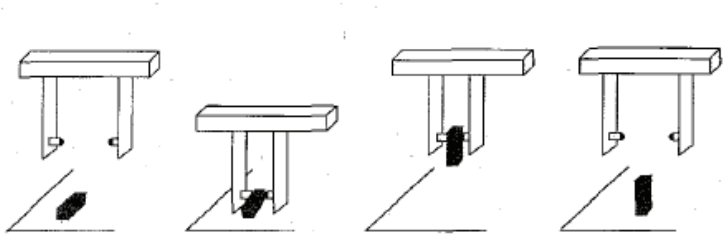

Figure 1.6: Pivot Grasp [3]

A more industrial approach to solving this problem is to attach an electrical rotary actuator to the end of a SCARA type robot to provide an added DOF. However, electrical rotary actuators require a separate drive controller from that of the robot. Motors may lead to significant downtime and added cost. Another option

is to attach a pneumatic rotary actuator to the end of a SCARA type robot to provide an added DOF. An example of a pneumatic rotary actuator is the Schunk SKE pneumatic swivel head shown in Fig. 1.7[3]. The Schunk SKE is a low weight three position pneumatic actuator geared clean environments such as assembly and packaging. Pneumatic rotary actuators offer less flexibility than electrical actuators as they can generally only travel to two or three positions.

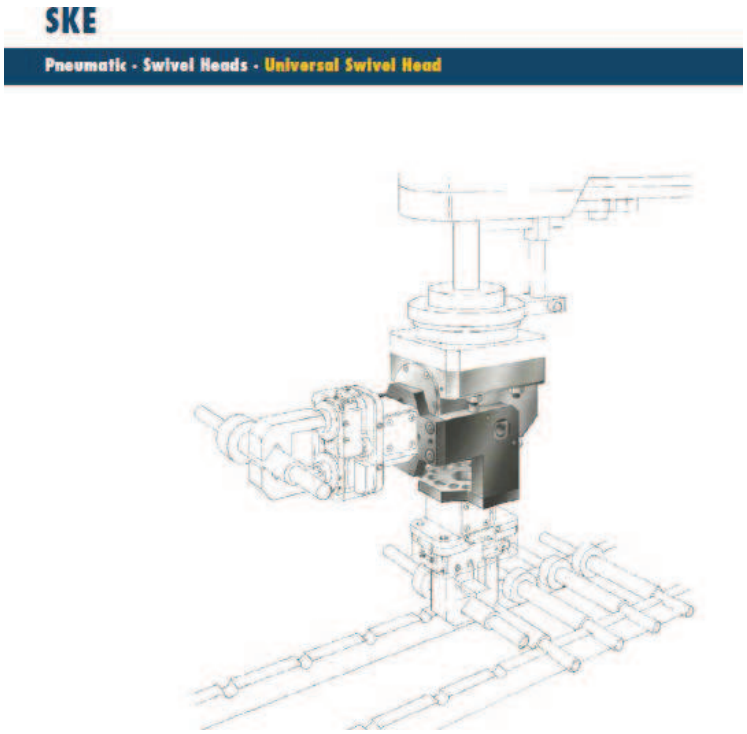

Figure 1.7: Schunk SKE Pneumatic Swivel Head

Researchers have also focused on underactuated systems that take advantage of the dynamics of the system to manipulate a part. Lynch and Mason [14] created a one DOF robot that manipulates a part by flipping it in the air and exploiting the dynamic effects. This work is intriguing, but it is not industrially feasible because it requires complex dynamic modeling as well as a complex control system. Additionally, it lacks robustness.

Lynch et al. also created a 3-DOF robot that exploits dynamic properties to control a passive joint [15]. Fig. 1.9 shows the 3-DOF system. The first two joints

[3]Figure 1.7 is used with permission from Schunk.

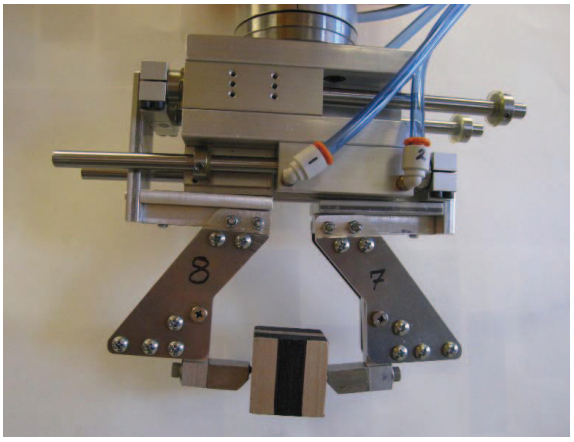

Figure 1.8: Metamorphic Gripper [13]

are active and the third joint is a passive joint. As shown this robot is in the horizontal plane. By moving the actuated joints appropriately the third passive joint will move to the desired position. One problem with this system is that not all trajectories are achievable at higher speeds. In addition, the dynamics change if the robot is oriented in the vertical plane or if there are changes with friction.

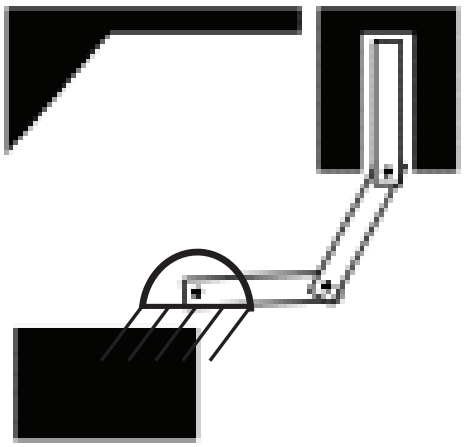

Figure 1.9: Underactuated Robot [15]

1.3 Summary

As was shown in this chapter there are two common approaches to the problem of orienting parts for an assembly task. These two approaches can be categorized into parts feeding systems and end-effector designs. End-effectors can further be categorized as complex anthropomorphic hands or simple binary

grippers. Complex anthropomorphic hands are not industrially feasible due to the coordination of all of the DOF, and simple grippers do not offer enough flexibility for an industrial assembly task. This research aims to simplify the part orientation problem by creating an industrially feasible end-effector that is both flexible and simple. The goal is to create an end-effector that provides an added DOF to a SCARA robot without adding significant complexity.

Chapter 2 will provide details of the mechanical design process. This will be followed by a kinematic analysis in Chapter 3. Next, a dynamic analysis of this system will be provided in Chapter 4. Following this analysis, Chapter 5 will focus on the end-effector manufacturing and testing. Finally, Chapter 6 will explore ideas for future work.

CHAPTER 2

Mechanical Design

This chapter outlines the design process as well as the decision making that occurred during the design process. This chapter begins with a section outlining the design requirements. Engineering requirements were then determined based on the design requirements. After determining the engineering requirements, a standard quality functional deployment process was used to determine the relationship between the engineering requirements and the design requirements. The next step in the design process was to complete the conceptual design. Once the final concept was chosen, different design configurations were created. The final step in the design process was to determine specific part dimensions.

2.1 Design Requirements

In this design five design requirements for the end-effector were chosen. The end-effector should be:

1. Robust: high number of cycles
2. Economical: low capital cost
3. Fast: short cycle time
4. Repeatable: low positioning error
5. Flexible: easily adaptable for different parts

To determine the relative weight of each design requirement a pairwise comparison was completed (Table 2.1). Each design requirement was compared to each of the other design requirements. When comparing two design requirements they are denoted with either a one or a zero. A one indicates a design requirement

of greater importance. This leads to a rough estimate of how important each design requirement is relative to the others. For instance, in Table 2.1 robust is compared to economical in the first column. It was thought that it was more important for the system to be economical than robust. Thus, a one was given for economical and a zero for robust. Robust was then compared against each of the other design requirements. The column labeled "Total" shows the total number of ones that each design requirement received. This can then be expressed as a percentage showing the relative importance of each of the design requirements. Table 2.1 shows that robustness is the most important design requirement and accuracy is the least important. However, the system should still be low cost, fast, and flexible. This table is inherently subjective, but it is useful because it shows that none of the design requirements can be ignored. Additionally, the table of importance weights is also used to evaluate different conceptual designs. This analysis will be completed in Section 2.4.

Table 2.1: Pairwise Comparison

Design Requirement													Total	Importance Weight
Robust	0	1	1	1									3	30%
Economical	1				0	1	0						2	20%
Fast		0			1			1	0				2	20%
Repeatable			0			0		0		1			1	10%
Flexible				0			1		1	0			2	20%

2.2 Engineering Requirements

For each of the design requirements there must be a quantitative way to measure how well a product performs a task. For instance, what is meant by "fast" or "repeatable?" The design requirements can be quantitatively measured by using engineering requirements.

Table 2.2 shows different engineering requirements that were considered for this design. It is used to help the designer determine which engineering requirements must be met to satisfy the design constraints. This is not meant to be an exhaustive list, but it will at least be used to help guide the design process.

Table 2.2: Engineering Requirements

Subfunction	Engineering Characteristic	Units	Limits
Robust	number of cycles	-	> 43200
Economical	number of custom parts	-	< 3
Fast	weight	N	< 4.45
	cycle time	s	< 2
	time to troubleshoot	min	< 5
Flexibility	range of motion	rad	$-\frac{\pi}{2}$ to $\frac{\pi}{2}$
Repeatability	positioning error	mm	$\pm$ 2.5
Simplicity	number of actuators	-	0

Each of the design requirements and the corresponding limits was chosen for a particular reason. The reasons for each choice are listed below:

- 43,200 cycles was chosen so that the robot could operate at 30 cycles per minute for 24 hours.
- The number of custom parts was chosen to be less than three to keep capital costs down. Specifically, this will keep machining costs low.
- A low weight of 4.45 N was chosen because it allows for heavier parts and grippers to be manipulated.
- A fast cycle time was critical in keeping costs down, and therefore a reasonable cycle time of 2 seconds was chosen. This is consistent with the robustness requirement.
- It should take less than five minutes to troubleshoot any problems that may occur during operation. This will lower costs by reducing the amount of downtime.
- The range of motion was limited to π rad. Typically, this is an acceptable range of motion for an assembly task.
- The device must be repeatable to within $\pm$2.5 mm.
- The number of actuators was chosen to be zero. This is important because it allows the end-effector to be controlled using the robot controller.

2.3 Quality Function Deployment

After the design requirements and engineering requirements are established it is possible to determine the relationship between them using a House of Quality. This information can be used to determine the relative weight of each of the engineering requirements. The results show that a lower overall weight is critical for a successful design. There are multiple reasons for this. A lighter end-effector corresponds to shorter cycle times, increased robustness, and lower cost. Additionally, a lighter end-effector allows a larger (in mass) part or gripper that may be attached to the end of a robot.

In this section the relationship between the design requirements and the engineering requirements was determined using a House of Quality. The next section will focus on the conceptual design phase. In this section different design concepts will be evaluated and one will be chosen to be developed further.

2.4 Conceptual Design

Conceptual design is perhaps the most important part of the design process. A design may be either doomed for failure or primed for success early on in the design process. Conceptual design is useful for analyzing alternative designs based on guiding physical principles. To aid this process a weighted rating method was used to evaluate different conceptual designs.

2.4.1 Magnet Device

The first design was based on the idea of locking and unlocking the rotational joint using a combination of magnets as well as inertial forces. Figure 2.1 shows a concept sketch of this device. A fixed stop is placed at an angle θ with respect to the vertical. As the robot accelerates the gripper would rotate until the two magnets touched. This would lock the gripper at a desired angle. After the assembly task is completed the robot would accelerate in the opposite direction, and the inertial forces would unlock the joint.

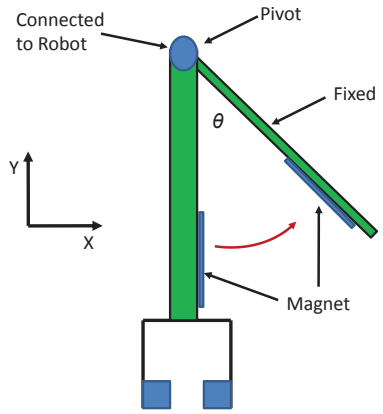

Figure 2.1: Magnet Concept

2.4.2 Ratchet Device

The second idea was to use a ratchet-like device in combination with inertial forces to continuously lock and unlock a rotational joint. As a ratchet is moved from one angle to another it becomes fixed at that angle. In this design the gripper of the robot would be attached to the end of a ratchet-like device. As the robot accelerates inertial forces would cause the ratchet, and therefore the gripper, to move to a desired angle.

2.4.3 Mechanical Brake

Another idea was to use a mechanical brake similar to a mechanical brake on a bicycle. It was thought that a similar idea could be used to stop the rotation of a pivoting gripper. The mechanical brake would be actuated using an additional pneumatic actuator.

2.4.4 Friction Device

Lastly, a device was considered in which controlled friction could be used to achieve the desired rotation. The controlled friction concept brought together the benefits from the other three concepts. The design is based on using positioning hinges (also called constant torque hinges) that provide a constant torque resistance throughout its range of motion. These types of hinges are identical to those generally used in laptops. Thus, when a user moves the screen of a laptop from one

angle to another the screen becomes fixed at that angle.

The idea is to apply the same concept to rotate a robotic gripper. Figure 2.2 shows the conceptual sketch for the controlled friction concept. As shown in the figure, a positioning hinge is attached to the end of the SCARA robot. The positioning hinge is attached to a pivot arm, and the pivot arm is attached to the gripper. If an external force presses against the pivot arm then the gripper will rotate. To provide an external force a fixed post is used. As the end of the robot moves from position 1 (Fig. 2.2a) to position 2 (Fig. 2.2b) the end of the robot moves along the $-x$-axis, and the pivot arm presses against the fixed post causing the gripper to rotate. This will provide the system with an added DOF. Thus, a four DOF SCARA type robot would have a selectable fifth DOF.

2.5 Concept Selection

Four different concepts were considered, but only one of these concepts could be developed further. To help determine which concept to develop further a weighted rating method was used. Table 2.3 shows how the weighted rating method was used to evaluate different conceptual designs. The four concept alternatives were rated on a scale from $0 - 4$ (Table 2.4) for each of the criteria. The rating is then multiplied by the importance weight to determine the weighted rating. The sum of the weighted ratings for each concept provides an overall rating for that concept. The results from Table 2.3 show that controlled friction idea achieved the highest score.

This type of analysis is inherently subjective. Therefore the designer should consider which concept alternative should be developed further. Three of the concepts had a "showstopper" that eliminated it from contention. For instance, the magnet idea was not chosen because it did not provide enough flexibility. While a ratchet-like device could be used to move the gripper to different angles while continually locking an unlocking, this device is difficult to manufacture and not very robust. The brake required the use of an additional actuator which adds significant overall complexity to the system. (The friction device did not have an obvious

showstopper, and therefore this was the device chosen for further development.)

Table 2.3: Weighted Rating Method

Criteria	Importance Weight	Magnetism		Ratchet		Mechanical Brake		Friction	
		Rating	WR	Rating	WR	Rating	WR	Rating	WR
Robust	30%	3	0.9	2	0.6	3	0.9	3	0.9
Economical	20%	3	0.6	3	0.6	1	0.2	3	0.6
Fast	20%	3	0.6	3	0.6	3	0.6	3	0.6
Repeatable	10%	4	0.4	2	0.2	3	0.3	3	0.3
Flexible	20%	1	0.2	4	0.8	4	0.8	4	0.8
		NA	2.7	NA	2.8	NA	2.8	NA	3.2

Table 2.4: Scale

Rating	Value
Unsatisfactory	0
Just Tolerable	1
Adequate	2
Good	3
Very Good	4

There are numerous other advantages to using this design. It was reasoned that the overall design would be lightweight due to the fact that there are few parts. This is important because a low weight will allow for heavier parts and end-effectors to be used. In addition, robust positioning hinges are readily available for purchase. This will allow for a low-cost device with a high degree of robustness and accuracy. Furthermore, it was thought that with proper path planning techniques the device would be repeatable to within the specified limits[1]. Lastly, the system is "flexible" in that any type of gripper may be attached to the pivot arm. This is an important concept for this design. Many times specialized grippers are designed to pick up a particular part. However, these specialized grippers are not designed to manipulate the part in any way. An advantage of the controlled friction concept is that specialized grippers may be still be utilized.

In this section four different conceptual designs were evaluated. The controlled friction concept was chosen to be developed based on the results of the weighted rating method as well as the fact that three of the designs had an obvious

[1]This will be explained in greater detail in Chapter 3.

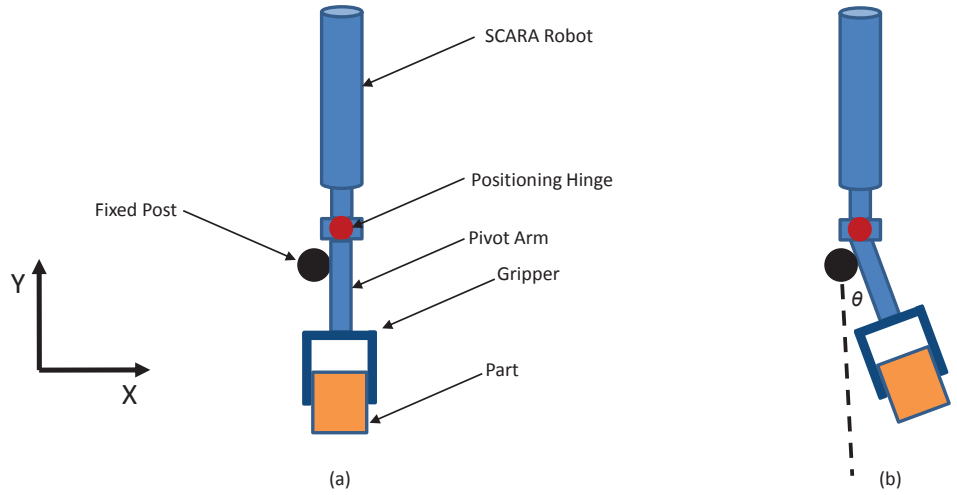

Figure 2.2: Concept Sketch: Friction may be used to maintain the gripper at a desired angle.

showstopper. The next section will focus on different configuration designs for the controlled friction concept.

2.6 Configuration Design

The next step in the design process is configuration design. The goal of configuration design is to determine the product architecture and part configuration. Product architecture refers to the number and type of components. Part configuration refers to how parts are spatially arranged and how they are connected [16].

Figure 2.3 shows the first configuration considered. In this configuration a pivot arm is attached to a positioning hinge. The positioning hinge is attached to a housing which is attached to the end of the robot. The gripper is attached to the pivot arm. While in theory this configuration could work, there were numerous issues with the configuration. The first is that the center of mass of the gripper is far away from the positioning hinge. Thus, an extremely strong positioning hinge would be required to to hold the gripper in place. Additionally, this configuration does not work well from a path planning perspective. This will be explained in greater detail in Chapter 3.

Figure 2.4 shows the second configuration considered. This configuration

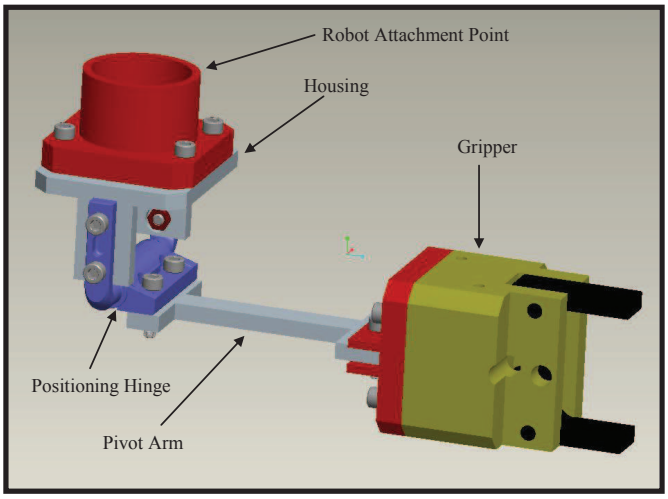

Figure 2.3: Configuration 1

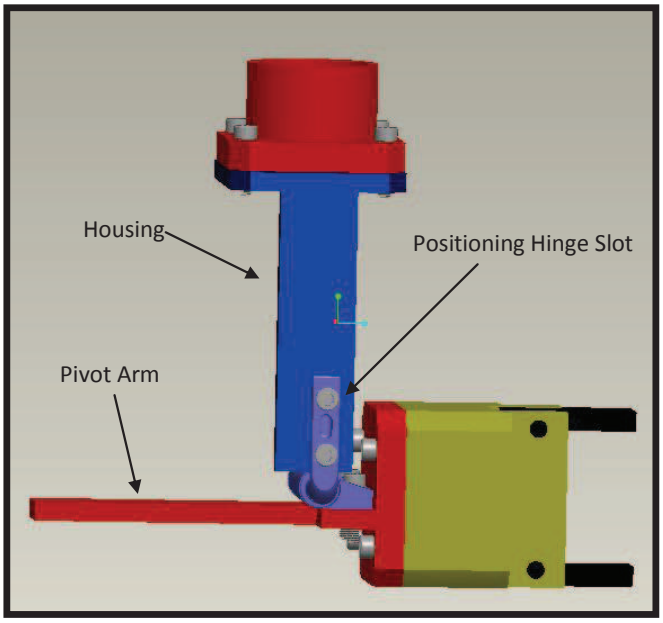

Figure 2.4: Configuration 2

improves upon the first in that the center of mass of the gripper is moved as close as possible to the positioning hinge. This means that the positioning hinge does not need to be nearly as strong as it would need to be for the first configuration. Another advantage of this configuration is that it works well from a path planning perspective. This will be explained in greater detail in Chapter 3.

The second configuration can be improved upon as shown in Fig. 2.5 (Configuration 3). In both configurations the housing and the pivot arm are the two

manufactured parts. First consider the housing. In configuration two, the positioning hinge slot is not centered with respect to the housing, but in configuration three it is centered with respect to the housing. Symmetry is important because it simplifies the design. The reason that the slot in configuration two is not symmetric to the housing is that it is desired that when the pivot arm is in the vertical position it aligns with the center axis of the robot attachment. This will simplify the path planning. Next consider the pivot arm. In configuration two the pivot arm is not centered over the positioning hinge. This is changed in configuration three by creating a housing around the positioning hinge. This creates a simplified design.

Configuration three was the final configuration chosen. The next step in the design process is to determine the exact dimensions of the end-effector. Some of the dimensions are chosen arbitrarily while other critical dimensions are chosen based on detailed analysis. The next section will outline which dimensions were critical dimensions and which dimensions were chosen arbitrarily.

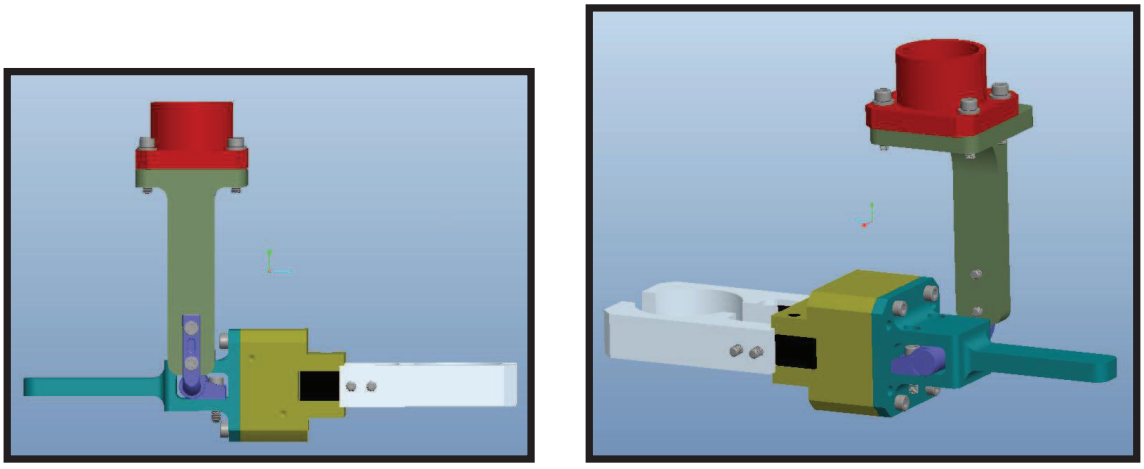

Figure 2.5: Configuration 3

2.7 Parametric Design

Parametric design [16] involves determining the design variables. Design variables are parameters of the design that are critical to the success of the design. The exact values of the design variables are determined using different analysis

techniques. Many of the dimensions on the two manufactured parts are not design variables. For instance, fillets were included in the design to reduce stress concentrations. The fillets were selected to be standard sizes (i.e., 0.3175 $\left(\frac{1}{8}\right)$ or 0.635 $\left(\frac{1}{4}\right)$ mm (in.)). These are not critical for the design. The critical dimension in this design is the distance L from the center of the positioning hinge to the end of the pivot arm as shown in Fig. 2.6.

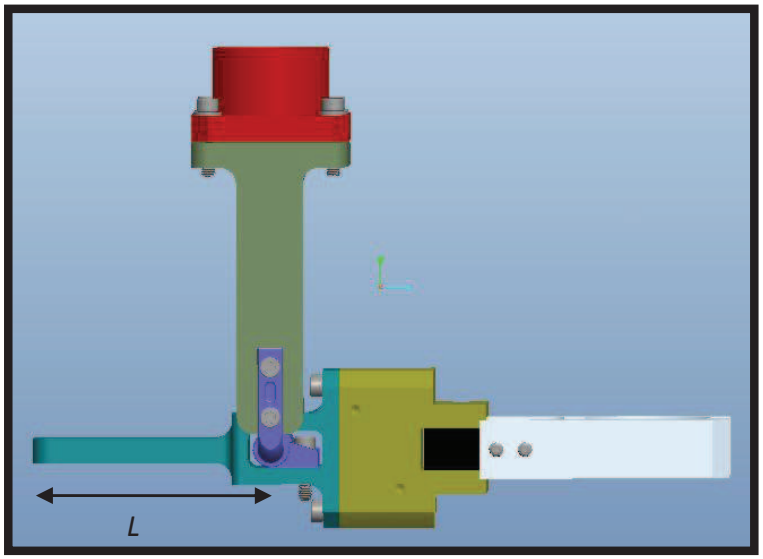

Figure 2.6: Critical Dimension

This dimension is critical because the success or failure of the design is based on choosing this dimension correctly. There are many design tradeoffs that need to be considered. There are multiple reasons why a designer would want the pivot arm to be as long as possible. A longer pivot arm:

1. reduces the external force required to rotate the gripper while still allowing for a strong positioning hinge. Thus, heavier grippers and parts can be accommodated which makes the system more flexible.

2. increases the positioning accuracy, as will be shown in Chapter 3.

3. allows for a greater range of motion in certain path planning techniques.

On the other hand, it is advantageous to have a shorter pivot arm. A shorter pivot arm:

1. reduces weight. Less material is needed both for the pivot arm as well as the housing.
2. increases rotation speed.
3. increases the available workspace of the robot.

As can be seen from the previous two lists, the length of the pivot arm is critical. Chapter 3 will be used to determine the appropriate length of the pivot arm with respect to different path planning techniques. Once the length of the pivot arm is chosen from a path planning perspective, a dynamic analysis will be completed in Chapter 4.

CHAPTER 3

Path Planning

There are many different aspects to motion planning for a robotic system. A common misconception is that motion planning involves only collision detection. However, in robotic assembly applications, motion planning may include the process of grasping the part, transferring the part, and positioning the part on a subassembly. Thus, both physical and geometrical constraints could be taken into account [17].

One subset of motion planning is path planning. Path planning considers the basic motion planning problem from a geometrical point of view. This means that the physical interaction between components is ignored (i.e., it is purely a kinematic problem). Thus, the friction forces between the pivot arm and the fixed post as well as the impact between the pivot arm and fixed post will be ignored.

This chapter outlines different path planning algorithms that can be used to achieve the desired gripper rotation. These algorithms are unique in that it is possible to use the built in controls from the robot to control the angle of rotation of the gripper. There is no need for any external control software. This is a distinct advantage over using an electrical rotary actuator.

3.1 Path Planning

Consider the schematic of the end-effector shown in Fig. 3.1. The purpose of the end-effector is to rotate the gripper around the z-axis by an angle θ. Positive θ is defined by the right hand rule (i.e., a counterclockwise rotation in the plane). As shown, the gripper is at $\theta = 0$. A cylindrical fixed post is positioned along the z-axis. As the end-effector of the robot moves in the xy-plane the pivot arm can be pressed against the fixed post which causes the positioning hinge, and thus the gripper, to rotate.

There are many different ways to move the robot's end-effector in the xy-plane to achieve a desired angle of rotation. However, depending on the application there are certain paths that are more suitable than others. The following sections outline different path planning algorithms that can be used for different assembly applications. In each of the different paths the center of the positioning hinge, point A, will be the point of interest. This is because this point is fixed relative to the end of the robot. In the following figures, a dotted line with an arrow will denote that the positioning hinge moves along that line.

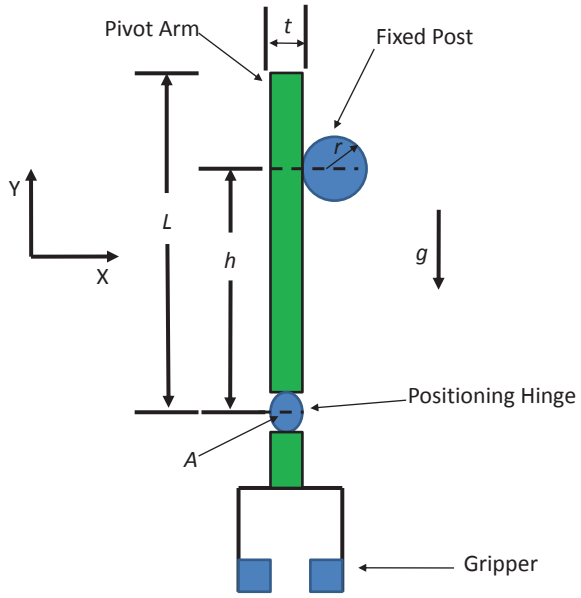

Figure 3.1: Pivoting Gripper Device Schematic

3.1.1 Horizontal Line Path

One way to achieve the desired rotation is to move the end-effector in a straight horizontal line path along the x-axis as shown in Fig. 3.2. As the end-effector moves along the x-axis the pivot arm makes contact with the fixed post and the force from the fixed post causes the positioning hinge to rotate. The desired angle of rotation is denoted as θ_f.

The main advantage to this path is that the gripper is rotated during normal operation of the robot. There is little wasted motion. Additionally, this path planning motion is time independent. There is, however, one distinct disadvantage

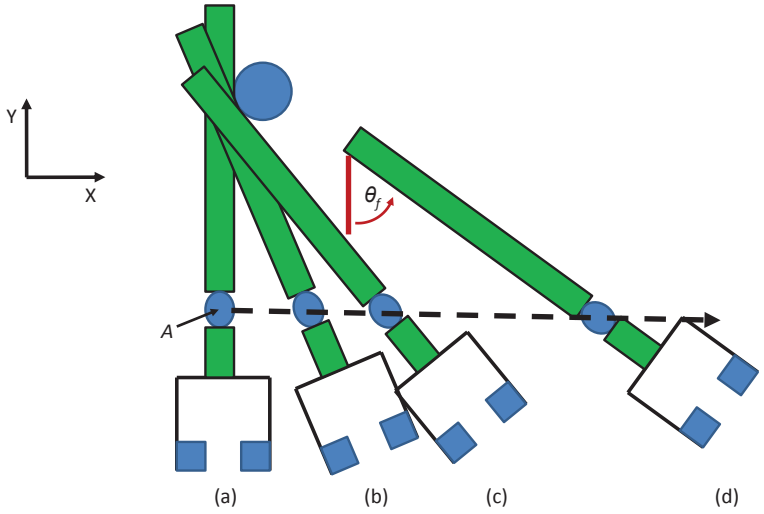

Figure 3.2: Horizontal Line Path

to this type of path planning; the gripper cannot be rotated a full 90° from the vertical position. There is a limit on the possible angle of rotation due to the diameter of the fixed post as well as geometrical constraints from the mechanical design. This will be explained further in the following sections.

3.1.2 45° Angle Path

As shown in the previous section, horizontal line path planning works well for certain assembly applications. However, many assembly tasks require the part be rotated 90° from a vertical position to a horizontal position. There are different ways to achieve this rotation. One possible path is to move the robot's end-effector at a 45° angle (relative to the y-axis) until the gripper has achieved the desired 90° rotation as shown in Figure 3.3.

The advantage to this path is that the gripper can be quickly pivoted from 0° to 90°. This angle is necessary for a wide variety of applications. For instance, consider the pick and place operation shown in Fig. 3.4 (Adapted from Goldberg et al. [4]). With a conventional SCARA robot the rectangular parts would need to be fed in their final upright configuration. At high feeding speeds this may cause the parts to topple over. However, with the ability to rotate the parts 90° from a horizontal to a vertical position the parts can be fed laying flat or vertically. This would allow for higher feeding speeds.

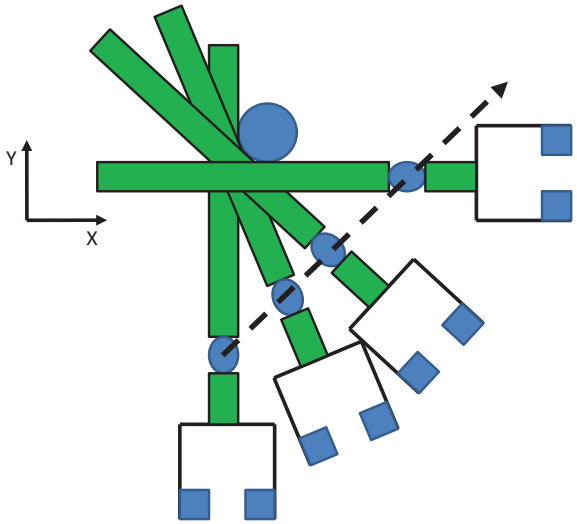

Figure 3.3: 45° Angle Path

The next section will outline another type of path in which the goal was to determine the shortest possible distance the robot's end-effector would need to travel to achieve the desired angle of rotation.

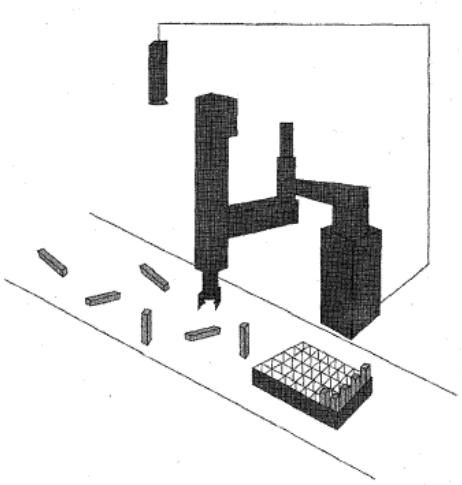

Figure 3.4: 90° Pick and Place [4]

3.1.3 Shortest Distance Path

The shortest distance path that is useful for certain assembly tasks. This is not necessarily the "best" path that works for every assembly operation. This path is called the shortest distance path because the goal was to determine the shortest possible distance the robot's end-effector would need to travel to achieve the desired

angle of rotation, θ_f.

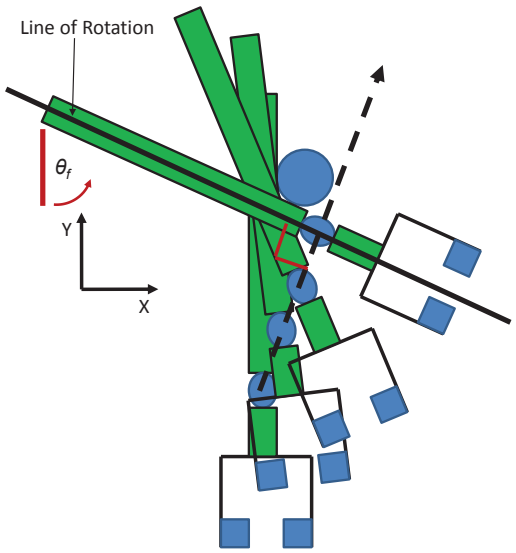

Figure 3.5: Shortest Distance Path

Consider the solid line that is at an angle of θ_f in Fig. 3.5. This line is fixed in space, and it will be denoted as the *line of rotation*. This line is offset and tangent to the fixed post. If the positioning hinge is moved from its initial position to any position on the line of rotation the gripper will be rotated by an angle θ_f. For example, the positioning hinge could move along a 45° line until it reaches the line of rotation. This is exactly what was proposed in the previous subsection.

The quickest way to achieve a rotation of θ_f is to move the positioning hinge from its initial position in a straight line perpendicular to the line of rotation. This type of motion, however, does have limits. For instance, it is impossible to rotate the gripper 90° using this type of motion. 90° rotation would correspond to moving the positioning hinge along the y-axis. Doing so would not provide any rotation.

Three different paths have been introduced in this section. The next section will provide the path planning algorithms that can be implemented in order to utilize the three different paths.

3.2 Path Planning Algorithms

This section presents the path planning algorithms for the different paths. For each of the path planning algorithms it is assumed the pivot arm begin in

contact with the fixed post at $\theta = 0$ (Fig. 3.6). Further, it is assumed that them location of the fixed post is known relative to the base frame of the robot. Thus, point $A(x_i, y_i)$ in Fig. 3.6 is the starting position of the center of the positioning hinge, and it is known relative to the fixed post and thus the base frame of the robot. The goal is to determine the final position $B(x_f, y_f)$ that the positioning hinge must be moved to in order to achieve the desired rotation θ_f.

The fixed post has a radius, r, and the pivot arm has a thickness t. The pivot arm length, h, is defined as the length from the center of the positioning hinge to the center of the fixed post. In this particular case, the rectangular shape of the pivot arm makes the geometry more difficult than is necessary. To simplify the geometry, the fixed post of radius r can be viewed as a circle of radius R where $R = r + \frac{t}{2}$. The pivot arm can then replaced by a line as shown in Figure 3.6.

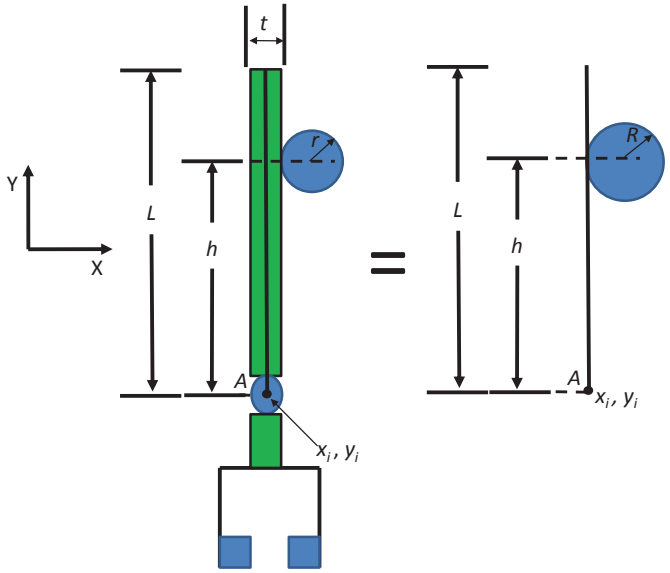

Figure 3.6: Simplified Geometry

3.2.1 Horizontal Line Path Algorithm

The horizontal line path algorithm is simple, but has limits on the possible angle of rotation. The reason for this is that there are geometrical constraints due to the mechanical design. In this type of motion the positioning hinge begins at a known point A and moves to point B along the x-axis. The kinematic equations governing this type of motion are

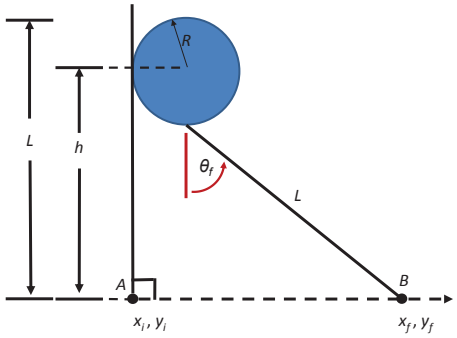

Figure 3.7: Horizontal Line Path Schematic

$$x_f = x_i + L\sin\theta_f + R \tag{3.1}$$

$$y_f = y_i. \tag{3.2}$$

In this analysis it is assumed that the end-effector is moved far enough along the x-axis that the top of the pivot arm completely moves past the fixed post as shown in Fig. 3.2(d). This is important because it allows for a shorter cycle time. The fixed post is a physical constraint. If the desired angle of rotation is achieved prior to the end-effector moving past the fixed post then the end-effector would need to be moved around or under the fixed post to continue motion along the x-axis. The excess motion of moving around or under the post would lead to higher cycle times.

The angle of rotation is dependent on both L and h. Thus,

$$L\cos\theta_f = h - R. \tag{3.3}$$

Solving for θ_f yields

$$\theta_f = \arccos\left(\frac{h-R}{L}\right). \tag{3.4}$$

Equation 3.4 shows that there are limitations on θ_f due to the constraints placed on h and L. In the chosen design $L = 8.9$ cm, $r = 0.41$ cm, and $R = 0.88$ cm. Due to the physical constraint of the housing that surrounds the positioning hinge, h must be at least 3.3 cm. In addition, for the max case it is desirable that the top of the

pivot arm aligns with the top of the fixed post. The reason for this is that it ensures that the pivot arm makes solid contact with the fixed post. Thus, h has a maximum value of $L - \frac{R}{2} = 8.46$ cm.

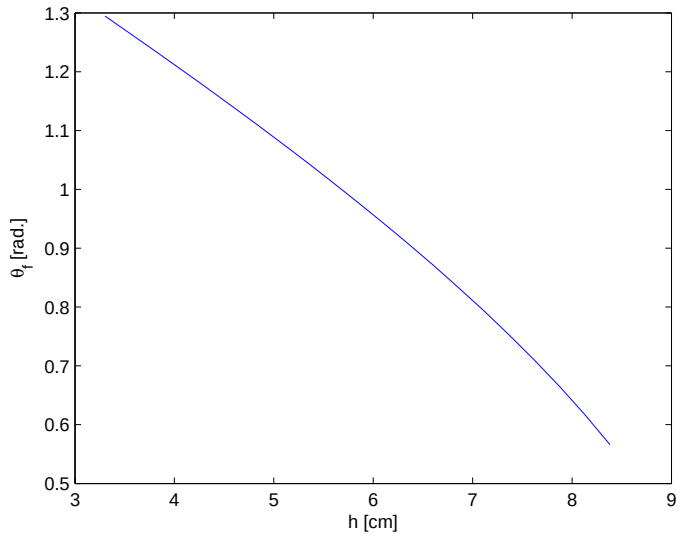

Figure 3.8: θ_f vs. h ($L = 8.9$ cm): The horizontal line path allows for a limited range of rotation.

Figure 3.8 shows how θ_f changes as a function of h with $L = 8.9$ cm. It can be seen from the plot that 0.54 rad. (31°) $< \theta_f <$ 1.29 rad. (74°) for horizontal line path motion. Figure 3.9 shows a plot of θ_f vs. h as L is varied from 5.1 cm to 24 cm in 1.27 cm increments. The line furthest to the left corresponds to $L = 5.1$ cm, and the farthest to the right is $L = 25.4$ cm. The dotted line is $L = 8.9$ cm. From Fig. 3.9 it is clear that the design follows the law of diminishing returns. That is, as L keeps increasing there is not a large increase in the range for θ_f. In fact, L would need to be increased to 25.4 cm to increase the range of θ_f by 20°. This is not realistic as L would be too long to be practical. Thus, a path planning algorithm is needed that allows for a full 90° rotation. This leads to the 45° path algorithm.

3.2.2 45° Path Algorithm

The 45° path is desirable because it provides a full 90° rotation. Figure 3.10 shows the schematic for straight line motion at a 45° angle ($\alpha = 45°$). The positioning hinge begins at a known point A and moves to an arbitrary point B

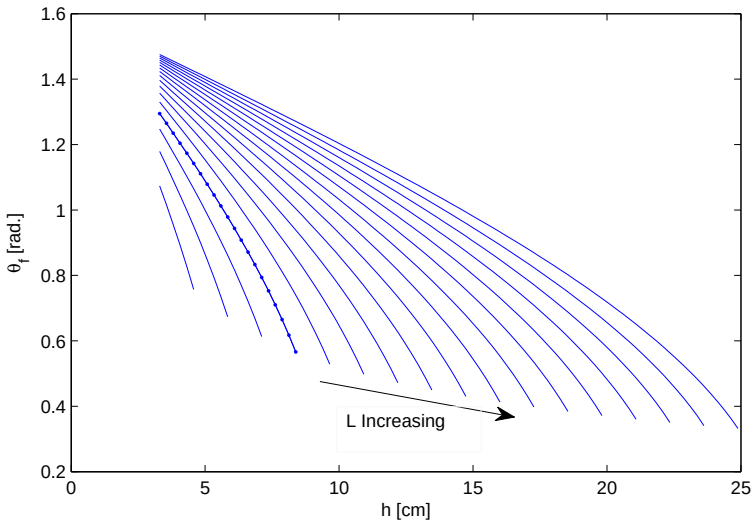

Figure 3.9: θ_f vs. h: The horizontal line path allows for a limited range of rotation.

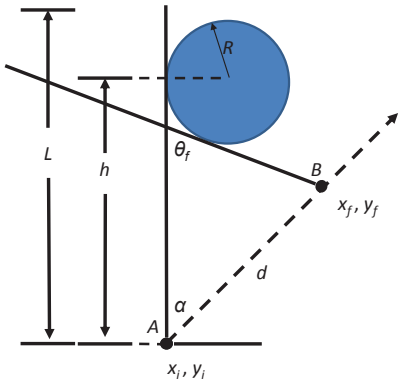

Figure 3.10: 45° Angle Schematic

along the 45° line. This leads to the following relationship between (x_i, y_i) and (x_f, y_f) for the 45° path.

$$x_f = x_i + d\sin\alpha \tag{3.5}$$

$$y_f = y_i + d\cos\alpha. \tag{3.6}$$

By analyzing the geometry from Fig. 3.10 the distance, d, from (x_i, y_i) to (x_f, y_f) in terms of h, R, α, and θ_f is

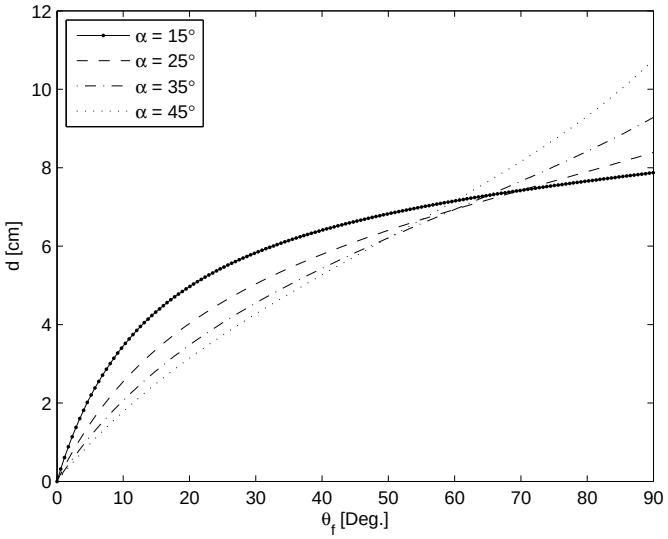

Figure 3.11: d vs. θ_f: Choosing $\alpha = 45°$ means that small changes in θ_f will not produce large changes in d.

$$d = \frac{\sin\theta_f}{\sin(\pi - \alpha - \theta_f)} \left(h - R\tan\frac{\theta_f}{2} \right). \tag{3.7}$$

Substituting $\alpha = 45°$ into Eqs. 3.5, 3.6, and 3.7 gives

$$x_f = x_i + d\frac{\sqrt{2}}{2} \tag{3.8}$$

$$y_f = y_i + d\frac{\sqrt{2}}{2} \tag{3.9}$$

$$d = \frac{\sin\theta_f}{\sin\left(\theta_f + \frac{\pi}{4}\right)} \left(h - R\tan\frac{\theta_f}{2} \right). \tag{3.10}$$

The full derivation for the expression in Eqn. 3.7 is given in Appendix A. Equation 3.10 shows that given the system parameters, θ_f, x_i, and y_i it is possible to use Equations 3.5 and 3.6 to quickly calculate the final position the end-effector of the robot must move to in order reach the desired rotation.

There are many different straight line paths that could have been chosen. However, there are specific reasons why $\alpha = 45°$ was chosen. Fig. 3.11 shows a plot of d vs. θ_f for different α where d is the distance from A to B as calculated in Eqn. 3.7. The $\alpha = 45°$ line has a relatively constant slope. This means that

throughout the range of motion small changes in θ_f will not produce large changes in d. Consider the $\alpha = 15°$ line in Fig. 3.11. As θ_f varies from $0° - 20°$, d varies from $0 - 4.98$ cm. Thus, a small change in θ_f produced a large change in d. Then, as θ_f varies from $20° - 90°$, d varies from $4.95 - 7.65$ cm. Thus, there is a large amount of rotation with very little change in d. This would cause the system to be more accurate during some parts of the cycle as opposed to others.

Additionally, a designer must be careful when choosing a value of α. By looking at Fig. 3.12 is it obvious that α must be greater than or equal to α_{min}. From Fig. 3.12

$$x = \sqrt{h^2 + R^2}, \tag{3.11}$$

and

$$\sin \frac{\alpha_{min}}{2} = \frac{R}{\sqrt{h^2 + R^2}}, \tag{3.12}$$

which leads to

$$\alpha_{min} = 2 \arcsin \frac{R}{h^2 + R^2}. \tag{3.13}$$

It is critical that $\alpha > \alpha_{min}$ because otherwise the positioning hinge will make contact with the fixed post.

3.2.3 Shortest Distance Path Algorithm

The shortest distance path algorithm can be derived in a similar fashion to that of the 45° path algorithm. Figure 3.13 shows the schematic for the shortest distance path. The goal of this algorithm is to determine the shortest possible distance the end-effector must be moved to achieve the desired rotation of θ_f.

From the geometry it can be shown that in the case of the shortest distance

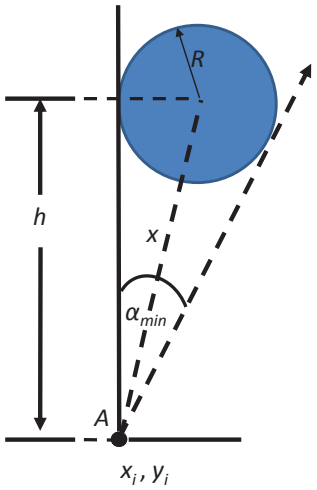

Figure 3.12: α_{min}: α must be $> \alpha_{min}$ to ensure the hinge does not make contact with the fixed post.

path equations

$$d = \frac{\sin\theta_f}{\sin(\pi - \alpha^\star - \theta_f)} \left(h - R\tan\frac{\theta_f}{2} \right). \tag{3.14}$$

Equation. 3.14 is identical to Eqn. 3.7 which was used to derive the 45° path algorithm. This leads to the following relationship between (x_i, y_i) and (x_f, y_f) for the shortest distance path:

$$x_f = x_i + d\sin\alpha^\star \tag{3.15}$$

$$y_f = y_i + d\cos\alpha^\star. \tag{3.16}$$

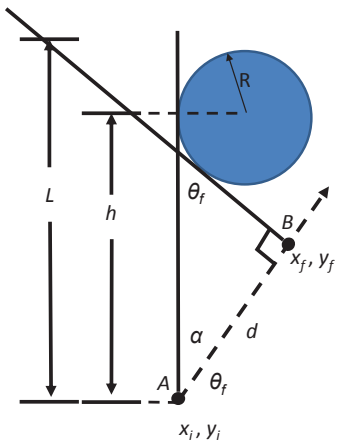

Figure 3.13: Shortest Distance Path Schematic

Substituting $\alpha^\star = \frac{\pi}{2} - \theta_f$ into the Eqs. 3.14, 3.15, and 3.16 gives

$$d = \sin\theta_f \left(h - R\tan\frac{\theta_f}{2} \right) \tag{3.17}$$

$$x_f = x_i + d\cos\theta_f \tag{3.18}$$

$$y_f = y_i + d\sin\theta_f. \tag{3.19}$$

3.2.4 Return Path

Each of the presented path planning algorithms provided a different way to rotate the gripper to a desired angle θ_f. However, once the gripper is at a desired angle there needs to be a path planning algorithm used to return the gripper to the $\theta = 0$ position. Just as there are numerous ways to achieve the initial gripper rotation, there are an infinite number of return path algorithms that could be used. In fact, the forward path algorithms can be implemented by using a matrix transformation. The algorithm presented here is useful for the situation in which the gripper must be returned to the same height as in the initial position.

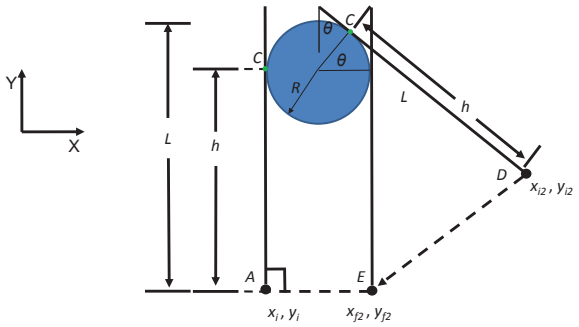

Figure 3.14: Return Path Schematic

In the return motion algorithm it is assumed that the gripper is at some angle, θ, with respect to the y-axis. In addition, it is assumed that the initial position occurs when point c makes contact with the fixed post. Point c is the point on the pivot arm that is a distance h from point A. This point was chosen because it allows for a large pivot arm. From the geometry shown in Fig. 3.14 the following

equations can be written for (x_{i2}, y_{i2}) and (x_{f2}, y_{f2}):

$$x_{i2} = x_i + R(1 + \cos\theta) + h\sin\theta \tag{3.20}$$

$$y_{i2} = y_i + h(1 - \cos\theta) + R\sin\theta \tag{3.21}$$

$$x_{f2} = x_i + 2R \tag{3.22}$$

$$y_{f2} = y_i. \tag{3.23}$$

Equations 3.20-3.23 show that the return algorithm is actually quite simple. It is a convenient way to return the gripper to the $\theta = 0$ position. One obvious disadvantage of this return path algorithm is that the gripper is now on the opposite side of the fixed post. Therefore, there needs to be a way to move the gripper either around or under the fixed post. Moving under the fixed post is not a good option. The reason is that there is not much clearance between the fixed post and the point where the pivoting device is connected to the robot. Moving around the fixed post (along the z-axis) is the better option. Figure 3.15 shows an example of how the end-effector can be moved from its final position to its initial position by moving around the fixed post.

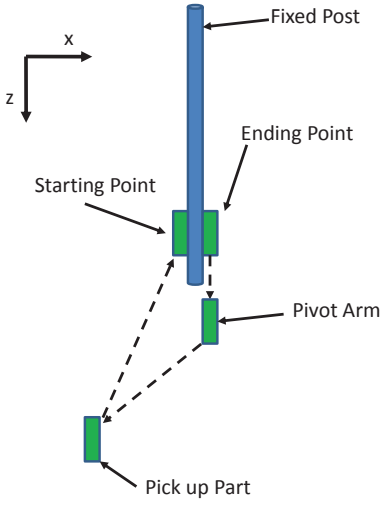

Figure 3.15: Return Path

In this situation the path planning algorithm depends on the particular operation. For instance, as shown in Fig. 3.15 the end-effector could be moved from its ending point to a point where another part may be picked up. It may then be

moved back to the starting point. There are countless ways to do this and one path may be better than another depending on the assembly operation.

In this chapter three different path planning algorithms were presented that may be used in conjunction with the end-effector to move a gripper to a desired angle. This was purely a kinematic analysis. Each of the three different path planning algorithms presented work well depending on the assembly operation. There is not one particular path that is the best for all situations. The next section will focus on the dynamics of the system. Specifically, a dynamic analysis will be completed to determine the necessary resistance torque of the positioning hinge.

CHAPTER 4

Dynamic Analysis

The positioning hinge is a critical part in the design. Different positioning hinges provide different levels of torque resistance. The hinge must provide enough torque resistance to resist inertial forces caused by rapid movements of the robot. This will ensure that the end-effector maintains its orientation once it has been moved to the desired angle. However, a positioning hinge with too much torque resistance would require a longer lever arm or larger post in order to limit the external forces acting on the robot. This is undesirable from a motion planning viewpoint.

In this chapter a standard dynamic analysis will be completed using Lagrange's equations to determine a closed form expression for the required resistance torque of the positioning hinge. The results will be verified by applying a Newton-Euler analysis for a few special cases. Lastly, the results of this analysis will be used to select the appropriate positioning hinge for different robotic assembly applications.

4.1 Lagrange's Equations of Motion

In this section the resistance torque of the positioning hinge, τ, is determined using Lagrange's equations of motion. τ is the torque needed to ensure the positioning hinge does not rotate due to inertial forces. It is assumed that all bodies are rigid and that the effects of gravity are included. Furthermore, it is assumed that the end-effector is attached to a four DOF SCARA robot (Fig. 4.1).

The general form of Lagrange's equation of motion with unconstrained

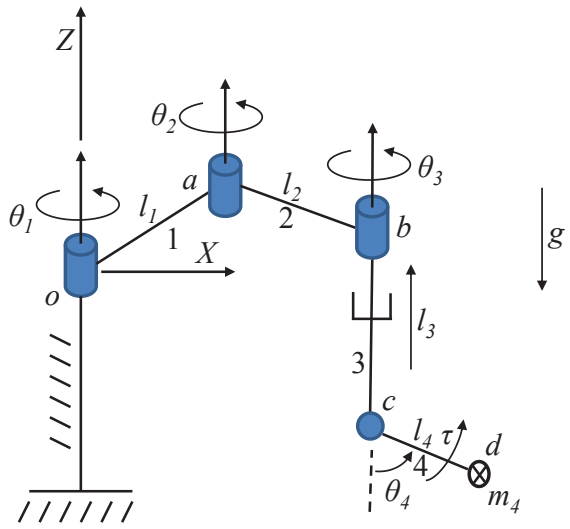

Figure 4.1: SCARA Robot with End-Effector

coordinates is

$$Q_i = \frac{d}{dt}\left(\frac{\partial L}{\partial \dot{q}_i}\right) - \left(\frac{\partial L}{\partial q_i}\right), \qquad i = 1, 2, ..., N, \tag{4.1}$$

where N is the number of generalized coordinates, Q_i contains the generalized forces, and q_i are the generalized coordinates [18]. The Lagrangian, L, can be written as

$$L = K - U \tag{4.2}$$

where K is the kinetic energy of the system and U is the potential energy of the system.

For this problem the number of generalized coordinates was chosen to be the same as the number of DOF of the system (i.e., the unconstrained case). The generalized coordinates are

$$\begin{aligned} q_1 &= \theta_1 \\ q_2 &= \theta_2 \\ q_3 &= \theta_3 \\ q_4 &= l_3 \\ q_5 &= \theta_4. \end{aligned} \tag{4.3}$$

The only generalized force that is of concern is the nonconservative moment acting on link 4 (i.e, the torque at the friction hinge). Thus, by substituting $Q_5 = \tau$, $q_5 = \theta_4$, and $\dot{q}_5 = \dot{\theta}_4$, into Eqn. 4.1 the resistance torque can be written as

$$\tau = \frac{d}{dt}\left(\frac{\partial L}{\partial \dot{\theta}_4}\right) - \left(\frac{\partial L}{\partial \theta_4}\right). \tag{4.4}$$

Eqn. 4.4 provides an equation for the amount of torque resistance required by the positioning hinge to overcome the inertial forces from the robot as well as gravity. This will ensure that the gripper will only be rotated when the pivot arm is pressed against the fixed post. This analysis will assume that all of the joints are defined or controlled ideally.

In general the kinetic and potential energy must be found for each link. However, in this particular case the kinetic and potential energy of links one through three can be ignored because the kinetic and potential energy terms are not dependent on either θ_4 or $\dot{\theta}_4$. For this system the Lagrangian can then be simplified to

$$L = K_4 - U_4. \tag{4.5}$$

The reference configuration for the system is shown in Fig. 4.2. There is an inertial coordinate system centered at o. The potential energy term for link four can be

determined by inspection as

$$U_4 = m_4 g l_4 (1 - \cos\theta_4). \tag{4.6}$$

The kinetic energy of link four can be expressed as

$$K_4 = \frac{1}{2} m_4 \|\vec{v}_d\|^2 + \frac{1}{2} \vec{\omega}_4^\top I_4 \vec{\omega}_4, \tag{4.7}$$

where I_4 is the inertia matrix of link 4, $\vec{v}_d$ is the velocity of the center of mass of the end-effector, and $\vec{\omega}_4$ is the angular velocity of the end-effector. The angular velocity of the end-effector can then be written in Eqn. 4.8 as

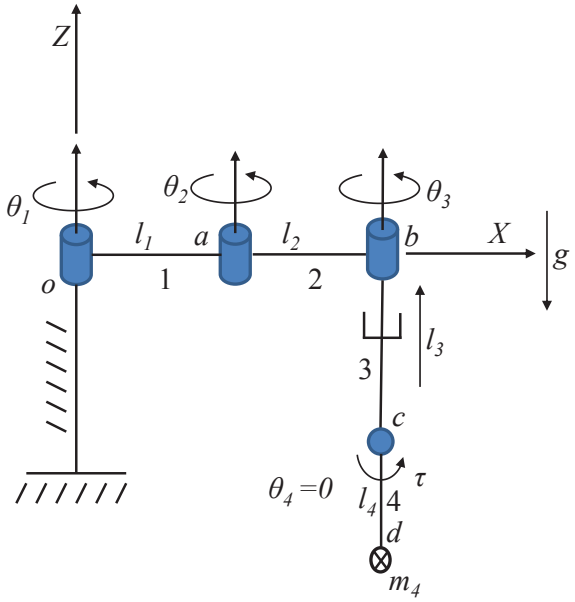

Figure 4.2: Reference Configuration

$$\vec{\omega}_4 = \dot{\theta}_4 s_{123} \hat{I} - \dot{\theta}_4 c_{123} \hat{J} + (\dot{\theta}_1 + \dot{\theta}_2 + \dot{\theta}_3) \hat{K}, \tag{4.8}$$

where $s_{123} = \sin(\theta_1 + \theta_2 + \theta_3)$ and $c_{123} = \cos(\theta_1 + \theta_2 + \theta_3)$. The final term that needs to be found is $\vec{v}_d$, the velocity of the center of mass of the end-effector. The

velocity of point d in component form can be expressed as:

$$\begin{aligned} v_{d_X} &= l_4\dot{\theta}_4 c_{123}c_4 - l_2 s_{12}(\dot{\theta}_1+\dot{\theta}_2) - l_1\dot{\theta}_1 s_1 - l_4 s_{123}s_4(\dot{\theta}_1+\dot{\theta}_2+\dot{\theta}_3) \\ v_{d_Y} &= l_4\dot{\theta}_4 s_{123}c_4 + l_2 c_{12}(\dot{\theta}_1+\dot{\theta}_2) + l_1\dot{\theta}_1 c_1 + l_4 c_{123}s_4(\dot{\theta}_1+\dot{\theta}_2+\dot{\theta}_3) \\ v_{d_Z} &= \dot{\theta}_3 + l_4\dot{\theta}_4 s_4. \end{aligned} \tag{4.9}$$

All of the variables for evaluating Eqn. 4.4 have now been defined. A MATLAB program was written to evaluate Eqn. 4.4 symbolically. A symbolic manipulator was used because of the complexity of the equations. By setting $\dot{\theta}_4 = 0$ and $\ddot{\theta}_4 = 0$ the equation for the torque resistance can be expressed as

$$\begin{aligned} \tau = l_4 m_4[(g+\ddot{l}_3)s_4 + c_4[l_1[\ddot{\theta}_1 s_{23} - \dot{\theta}_1^2 c_{23}] + l_2[s_3(\ddot{\theta}_1+\ddot{\theta}_2) - c_3(\dot{\theta}_1^2+\dot{\theta}_2^2)] \\ -l_4 s_4[(\dot{\theta}_1^2+\dot{\theta}_2^2+\dot{\theta}_3^2) + 2\dot{\theta}_3(\dot{\theta}_1+\dot{\theta}_2)] - 2\dot{\theta}_1\dot{\theta}_2(l_2 c_3 + l_4 s_4)]]. \end{aligned} \tag{4.10}$$

Equation 4.10 is important from a design perspective. Given the robot joint angles, velocities, and accelerations it is possible to create a torque profile showing the required resistance torque necessary so that the end-effector does not move due to inertial forces and gravity. By using Eqn. 4.10, a designer can select an appropriate positioning hinge for their particular assembly task.

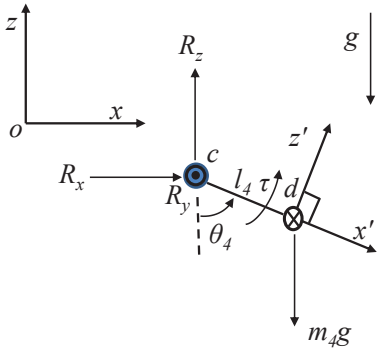

Figure 4.3: Free Body Diagram, Vertical Motion Case

4.2 Newton-Euler Equations of Motion

In this section a standard Newton-Euler dynamic analysis will be used to check the results obtained in Eqn. 4.10. A complete derivation would be very complex; therefore, three different limiting subcases will be examined and then compared to the results from the Lagrange formulation.

4.2.1 Vertical Motion

The first will be the limiting case in which the end-effector is being accelerated in the vertical direction against gravity. This is a common motion in many assembly tasks. The free body diagram (FBD) is shown in Fig. 4.3. In this case the forces include the reaction forces at the hinge, the weight of the end-effector, and the resistance torque of the positioning hinge, τ. Principal body fixed $x'y'z'$ axes were chosen with the origin located at the center of mass of the system (point d). Space fixed XYZ axes were chosen with origin at o.

The linear acceleration is:

$$\vec{a}_d = a_z\hat{k}. \tag{4.11}$$

The force equations can be written according to Newton's second law

$$\begin{aligned} \sum \vec{F} &= m\vec{a}_d, \\ \sum \vec{F}_x &= R_x c_{123} + R_y s_{123} = 0, \\ \sum \vec{F}_y &= -R_y c_{123} + R_x s_{123} = 0, \\ \sum \vec{F}_z &= R_z - m_4 g = m_4 a_z. \end{aligned} \tag{4.12}$$

Solving the force equations for R_x, R_y, and R_z shows that

$$\begin{aligned} R_x &= 0, \\ R_y &= 0, \\ R_z &= m_4(g + a_z). \end{aligned} \tag{4.13}$$

Summing the moments around the y'-axis yields

$$\sum \vec{M}_{y'_d} = -\tau + l_4 R_x \cos\theta_4 + l_4 R_z \sin\theta_4 = I_{y'y'_4}\ddot{\theta}_4. \tag{4.14}$$

Setting $\ddot{\theta}_4 = 0$ and substituting in R_x, R_z and $a_z = \ddot{l}_3$ into Eqn. 4.14 yields

$$\tau = m_4(g + \ddot{l}_3) l_4 \sin\theta_4. \tag{4.15}$$

Equation 4.15 is an expression for the torque resistance the positioning hinge must provide when the system is being accelerated in the $\hat{k}$ direction against gravity, and this result matches the results from Eqn. 4.10. As expected, the maximum torque occurs at $\theta_4 = \frac{\pi}{2}$ rad. The robot that the end-effector will be tested on has a maximum vertical acceleration of $8\frac{m}{s^2}$. This leads to a maximum torque value of approximately 2.3 N-m. However, this torque value is only for one particular case.

4.2.2 Rotation about the θ_3 Axis

The second limiting case is where the end-effector is rotating around the θ_3 axis. This is also a common motion used in assembly tasks. It is assumed that $\theta_1 = \theta_2 = \theta_3 = 0$, $\dot{\theta}_1 = \dot{\theta}_2 = 0$, and $\ddot{\theta}_3 = 0$. The FBD for this case is shown in Fig. 4.4. Summing the forces in the x and z directions yields

$$\begin{aligned} \sum \vec{F} &= m\vec{a}_d, \\ \sum \vec{F}_x &= R_x = m_4(-l_4 \sin\theta_4)\dot{\theta}_3^2, \\ \sum \vec{F}_z &= R_z - m_4 g = 0. \end{aligned} \tag{4.16}$$

Writing the moment equation around the y'-axis yields

$$\sum \vec{M}_{y'_d} = -\tau + R_x l_4 \cos\theta_4 + R_z l_4 \sin\theta_4 = I_{y'y'_4}\ddot{\theta}_4. \tag{4.17}$$

Setting $\ddot{\theta}_4 = 0$, substituting R_x and R_z from Eqn. 4.16 into Eqn. 4.17, and solving for τ yields the equation for the resistance torque when the end-effector is being

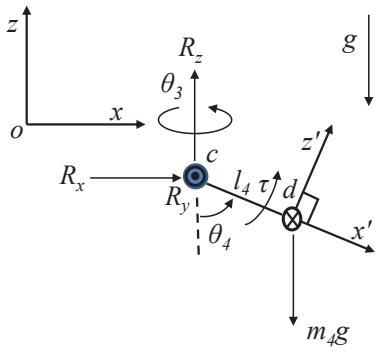

Figure 4.4: Free Body Diagram, Rotation about the θ_3 Axis

rotated around the θ_3 axis,

$$\tau = m_4 l_4 \sin\theta_4 (g - l_4 \cos\theta_4 \dot{\theta}_3^2). \tag{4.18}$$

This expression matches the results obtained from the Lagrange formulation in Eqn 4.10.

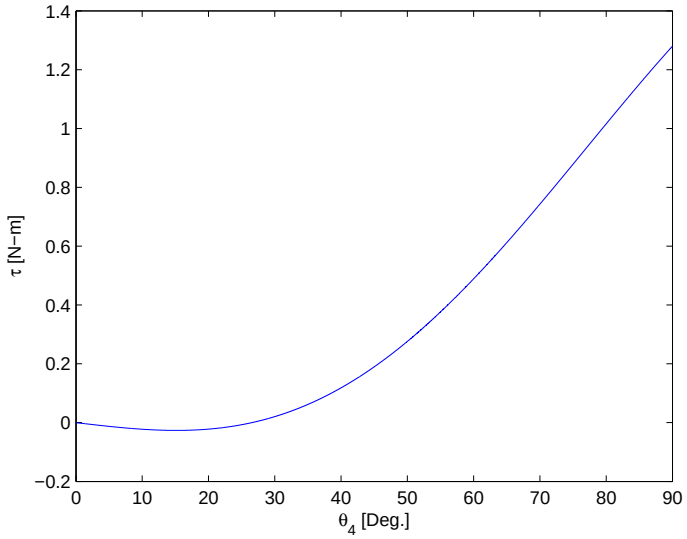

Figure 4.5: τ vs. θ_4 for θ_3 rotation

Figure 4.5 shows a plot of τ vs. θ_4 for constant rotation about the θ_3 axis at 10.5 $\frac{\text{rad}}{\text{s}}$. Even at such a high speed of rotation it is clear from Fig. 4.5 that the torque on the system due to the weight of the end-effector dominates the centrifugal acceleration. It should also be noted that the maximum torque value is approximately 1.2 N-m which is less than the 2.3 N-m of torque required motion

along a vertical axis.

4.2.3 Rotation about the θ_1 Axis

The third limiting case is where the end-effector is moving in circular motion around the θ_1 axis. It is assumed that $\theta_1 = 0$ rad, $\theta_2 = 0$ rad, and $\theta_3 = \frac{\pi}{2}$ rad. Additionally, $\dot{\theta}_2 = \dot{\theta}_3 = \ddot{l}_3 = 0$, $\ddot{\theta}_1 = 3\ \frac{\text{rad}}{\text{s}^2}$, and $\dot{\theta}_1 = 4.36\ \frac{\text{rad}}{\text{s}}$. $\ddot{\theta}_1$ and $\dot{\theta}_1$ were chosen based on the maximum angular acceleration and velocity of joint 1 of the robot.

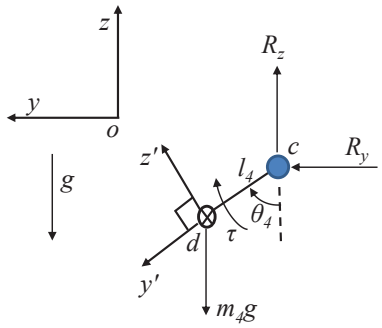

Figure 4.6: Free Body Diagram, Rotation about the θ_1 Axis

The derivation for this case will follow a similar pattern as the previous two cases. The FBD for this case is shown in Fig. 4.6. Summing the forces in the z and y direction yields

$$\begin{aligned} \sum \vec{F}_z &= R_z - m_4 g = m_4 a_{d_z}, \\ \sum \vec{F}_y &= R_y = m_4 a_{d_y}. \end{aligned} \tag{4.19}$$

In order to evaluate Eqn. 4.19 it is necessary to determine the acceleration of the center of mass (point d). The acceleration of the center of mass can be expressed in Eqn. 4.20 as

$$\vec{a}_d = \vec{a}_c + \vec{a}_{rel} + \vec{\alpha}_{cd} \times \vec{r}_{c/d} + \vec{\omega}_{cd} \times (\vec{\omega}_{cd} \times \vec{r}_{c/d}) + 2\vec{\omega}_{cd} \times \vec{v}_{rel} \tag{4.20}$$

Because points c and d are on the same rigid body there is no relative velocity or

relative acceleration. The remaining terms can be expressed as follows

$$\begin{aligned} \vec{a}_c &= -(l_1+l_2)\dot{\theta}_1^2\hat{i} + (l_1+l_2)\ddot{\theta}_1\hat{j}, \\ \vec{\alpha}_{cd} &= \ddot{\theta}_1\hat{k}, \\ \vec{r}_{c/d} &= l_4\sin\theta_4\hat{j} - l_4\cos\theta_4\hat{k}. \end{aligned} \tag{4.21}$$

Substituting Eqn. 4.21 into Eqn. 4.20 yields the acceleration of point d given in Eqn. 4.22 as,

$$\vec{a}_d = (-l_4\sin\theta_4\ddot{\theta}_1 - (l_1+l_2)\dot{\theta}_1^2)\hat{i} + ((l_1+l_2)\ddot{\theta}_1 - l_4\sin\theta_4\dot{\theta}_1^2)\hat{j}. \tag{4.22}$$

Substituting $\vec{a}_{d_y}$ and $\vec{a}_{d_z}$ into Eqn. 4.19 and solving for the reaction forces gives

$$\begin{aligned} R_z &= m_4 g, \\ R_y &= m_4[(l_1+l_2)\ddot{\theta}_1 - \dot{\theta}_1^2 l_4\sin\theta_4]. \end{aligned} \tag{4.23}$$

The moment equation around the x'-axis can then be written as:

$$\sum \vec{M}_{x'd} = \tau - m_4[(l_1+l_2)\ddot{\theta}_1 - \dot{\theta}_1^2 l_4\sin\theta_4]l_4\cos\theta_4 - m_4 g l_4\sin\theta_4 = 0. \tag{4.24}$$

Finally, solving for τ gives

$$\tau = m_4[(l_1+l_2)\ddot{\theta}_1 - \dot{\theta}_1^2 l_4\sin\theta_4]l_4\cos\theta_4 + m_4 g l_4\sin\theta_4. \tag{4.25}$$

The expression for τ in Eqn. 4.25 matches the expression determined using Lagrange's equations in Eqn 4.10. Figure 4.7 shows how the required positioning hinge torque varies as θ_4 is varied from 0° to 90°. Recall that this is this is the case in which $\ddot{\theta}_1 = 3\ \frac{\text{rad}}{\text{s}^2}$, $\dot{\theta}_1 = 4.36\ \frac{\text{deg.}}{\text{s}}$, and $\theta_3 = \frac{\pi}{2}$ rad. From Fig. 4.7 the maximum torque is approximately 2.2 N-m. This is actually less than the torque required to accelerate the end-effector in the vertical direction against gravity. However, this is not true if θ_3 is changed from 90° to 0°. In this case there is a large centrifugal acceleration. Figure 4.8 shows that with $\theta_3 = 0$ the max torque required is

approximately 12 N-m. Simply rotating θ_3 by 90° caused the required torque to increase by a factor of 5. This example shows that with careful path planning the amount of torque required by the positioning hinge can be reduced significantly.

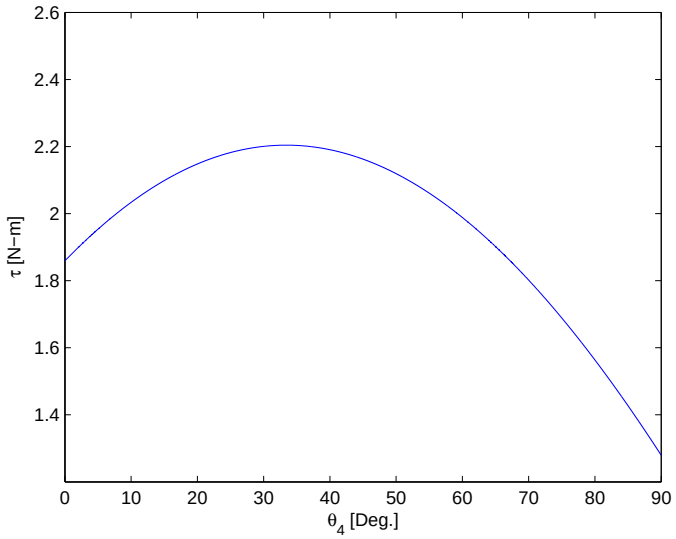

Figure 4.7: τ vs. θ_4 for θ_1 rotation ($\theta_3 = 90°$)

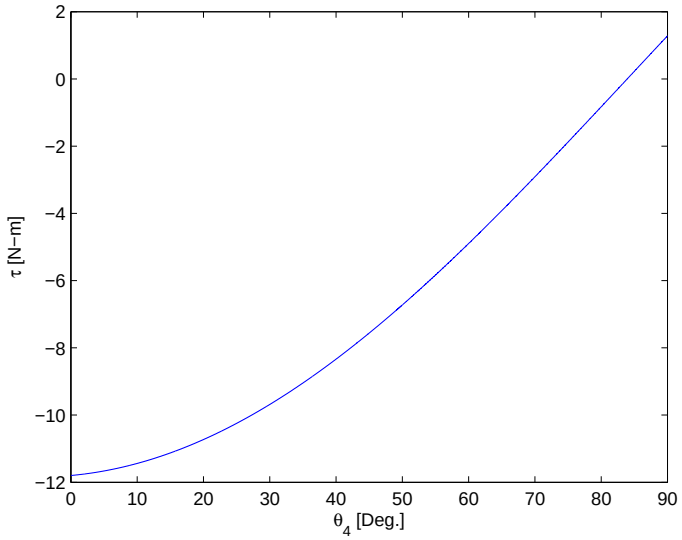

Figure 4.8: τ vs. θ_4 for θ_1 rotation ($\theta_3 = 0°$)

The purpose of this research is to prove that this device is feasible. Thus, the simplest type of motion (horizontal motion) will be used for testing. Figure 4.9 shows a plot of the torque resistance required for horizontal motion. This plot shows

that the required torque for horizontal motion is approximately 1 N-m. Therefore, for the experimental testing a positioning hinge with at least 1 N-m of torque must be used so that the gripper does not rotate due to inertial forces. The end-effector can still be moved in the vertical direction or in circular motion. However, with a 1 N-m positioning hinge these movements can't be made at the max speed of the robot. The advantage of the results of Eqn. 4.10 is that one can calculate exactly how fast the robot can move before movement of the end-effector occurs. Table 4.1 shows the maximum allowable accelerations and velocities that can be used with a 1.5 N-m hinge. 1.5 N-m is used because this is the amount of torque the chosen positioning hinge provides.

Table 4.1: Maximum Accelerations and Velocities

Case	Variable	Max Value
Vertical Motion	$\ddot{l}_3$	2 $\frac{\text{m}}{\text{s}^2}$
Rotation about the θ_3 Axis	$\dot{\theta}_3$	10.47 $\frac{\text{rad}}{\text{s}}$
Rotation about the θ_1 Axis ($\theta_3 = \frac{\pi}{2}$ rad)	$\ddot{\theta}_1$	1.5 $\frac{\text{rad}}{\text{s}^2}$
Rotation about the θ_1 Axis ($\theta_3 = 0$ rad)	$\dot{\theta}_1$	1.57 $\frac{\text{rad}}{\text{s}}$

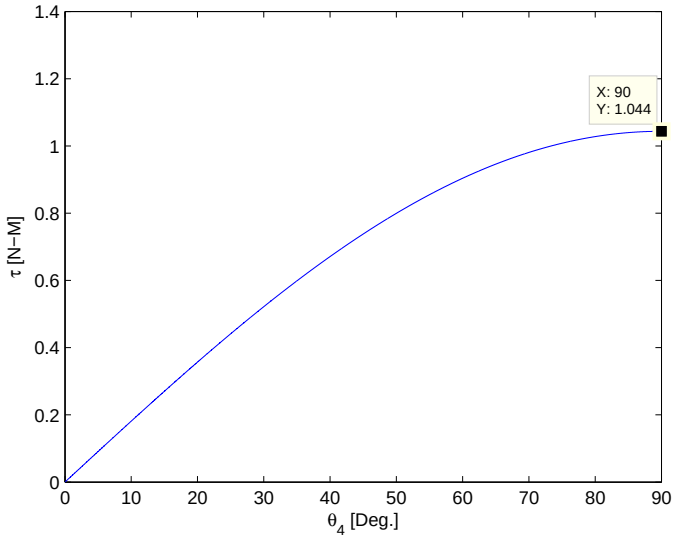

Figure 4.9: τ vs. θ_4 for Horizontal Motion

In this chapter an equation for the required resistance torque of the positioning hinge was derived using Lagrange's equations of motion. This closed form solution is a valuable design tool. Three special cases were derived using

Newton's equation of motion. It was seen from the examples that with careful path planning the amount of required torque can be reduced significantly. This is extremely valuable. By reducing the torque requirements of the positioning hinge heavier grippers and parts can be attached to the end-effector. With the kinematic and dynamic analysis complete, the next step in the design process was manufacture and test the end-effector. This process will be outlined in Chapter 5.

CHAPTER 5

End-Effector Manufacturing and Testing

This chapter will cover a range of topics related to the manufacturing and testing of the end-effector. This chapter begins with a section covering the material selection process. Different materials were compared based on their mechanical properties. After explaining the material selection process, there will be a section in this chapter that details how the specific positioning hinge was chosen. Finally, this chapter will outline different experimental tests that were performed. This includes tests done on a rapid prototype as well as the final product.

5.1 Material Selection

An important part of any design is the material selection. There are different classes of materials such as metals, polymers, or composites. From the onset of the material selection process it was decided that the end-effector should be made out of metal. The reason for this is that metals are typically stiff, impact-resistant, and easily machined. Using metal will allow for a more robust system. The two types of metals considered were steel and aluminum. Other metals such as copper or titanium were not considered because these materials were either too costly or had undesirable material properties. For instance, copper was not considered because it is too soft and not as easily machined as either steel or aluminium.

The most important factor considered when choosing between steel and aluminium was the density of the material. Both steel and aluminum are stiff enough for this application, and so density was considered to be the critical factor. However, either metal could be used in the design. Steel has a density of 7.75 $\frac{g}{cm^3}$ whereas aluminum has a density of 2.27 $\frac{g}{cm^3}$. Thus, using aluminum instead of steel reduces the weight by 64% assuming the same part geometry. As was seen in Chapter 2 a low weight is important for the design. The combined weight of the

pivot arm and the base using aluminium is 3.11 N. This is in contrast to a combined weight of 8.77 N for steel. This end-effector was designed to be attached to a robot with a payload of 34.3 N. This means that saving 5.7 N allows for added flexibility in either the part weight or gripper weight.

There were other material properties considered as well. Impact strength and fatigue strength were also considered. Steel has a better fatigue strength and impact strength. However, it was thought that a lower weight end-effector was more important than either fatigue strength or impact strength. After choosing an appropriate material, it was necessary to choose an appropriate positioning hinge.

5.2 Positioning Hinge Selection

There are many different types of commercially available positioning hinges. These hinges come in many different shapes. There are standard hinges, L-shaped hinges, U-shaped hinges, and others. During the configuration design phase discussed in Chapter 2, it was determined that an L-shaped hinge should be used. The chosen hinge also had to satisfy certain engineering requirements. The three most important specifications of the hinge were the torque resistance, springback, and number of cycles. After a thorough search for different positioning hinge manufacturers it was determined that the hinge would be purchased from Reell. The chosen hinge (Fig. 5.1)[1] was the Reell PHK positioning hinge with 1.5 N-m of torque resistance. The PHK hinge has a steel shaft that is surrounded by clips. One part of the hinge is attatched directly to the shaft. The other part of the hinge is connected to the clips. When the hinge is rotated the clip/shaft interference provides the necessary torque.

This hinge was chosen for multiple reasons as listed below:

- The hinge is available in five different levels of torque resistance ranging from 1.5 N-m to 5.5 N-m. Thus, a stronger or weaker positioning hinge may be used depending on the part weight or gripper weight attached to the end-effector.

[1]Figure 5.1 is used with permission from Reell Precision Manufacturing, Inc.

Figure 5.1: Reell PHK Positioning Hinge

- The hinge allows for a full 360° of rotation. This allows the gripper to operate in the specified range of −90° and 90°.
- This hinge has a life of 20,000 cycles. This is less than the desired 43,200 cycles, but after much searching this was the most robust hinge available.
- The typical springback is less than 1°. This should allow for the desired positioning accuracy and repeatability.

One drawback from this hinge is that the torque tolerance is ±20% of the nominal torque. Therefore, a positioning hinge with 1.5 N-m of torque operates in a range of 1.2 N-m to 1.8 N-m. This means that the designer has to be extremely careful in choosing a positioning hinge with the appropriate torque. For this design a hinge with 1.5 N-m of torque was chosen. There are two reasons for this. The first was that the dynamic analysis from Chapter 4 showed that the hinge required at least 1 N-m of torque for horizontal motion. The 1.5 N-m positioning hinge satisfies this requirement. The second reason for choosing this hinge is that this hinge was first going to be used with plastic parts made from the rapid prototyping machine in the Marquette University machine shop. Testing the device with plastic is much different than with metal. The main concern was that if the positioning hinge was too strong the pivot arm would break before being able to overcome the torque resistance of the hinge.

The final deciding factor in choosing this hinge was the cost. Part of the goal of this research is to create a low-cost system. Table 5.1 shows the approximate costs of each of the components in this design. With a low cost positioning hinge and only two manufactured parts, this is an extremely low cost end-effector. The

labor cost is an estimate of the cost to manufacture one set of parts. If these types of grippers were mass produced the costs of this system would be reduced significantly. Once the positioning hinge was selected, the next step was to build and test the end-effector.

Table 5.1: Costs

Component	Cost ($)
Reel PHK Positioning Hinge	50
Material	100
Labor	1000
Assorted Bolts	0.50

5.3 Detail Design

During the parametric design phase it was determined that the distance, L, from the center of the positioning hinge to the tip of the pivot arm was critical to the success of this design. This dimension was chosen to be 8.9 cm. The reason for this is that this value allows for a wide range of rotation with the straight line path algorithm discussed in Chapter 3. Additionally, at this length both the 45° path algorithm and the shortest distance path algorithm can be utilized effectively.

Figure 5.2 shows a detailed drawing of the pivot arm. There are certain features worth pointing out. The first is that fillets can be seen throughout the design which help to reduce stress concentrations. The second important feature is that there is a housing that surrounds the positioning hinge. As mentioned in Chapter 3, careful path planning is required to ensure that the fixed post does not jam into the housing.

Figure 5.3 shows a detailed drawing of the base. One important feature of the base is the slot that the positioning hinge sits in. This slot helps to ensure that the side of the positioning hinge does not rotate. By looking at the top view one will notice that the four attachment holes are not centered. The reason is that it was desired that the pivot arm be centered with respect to the attachment point of the robot. When the pivot arm is at $\theta = 0°$ the center axis of the pivot passes through the center axis of the robot attachment point (the large hole in the top

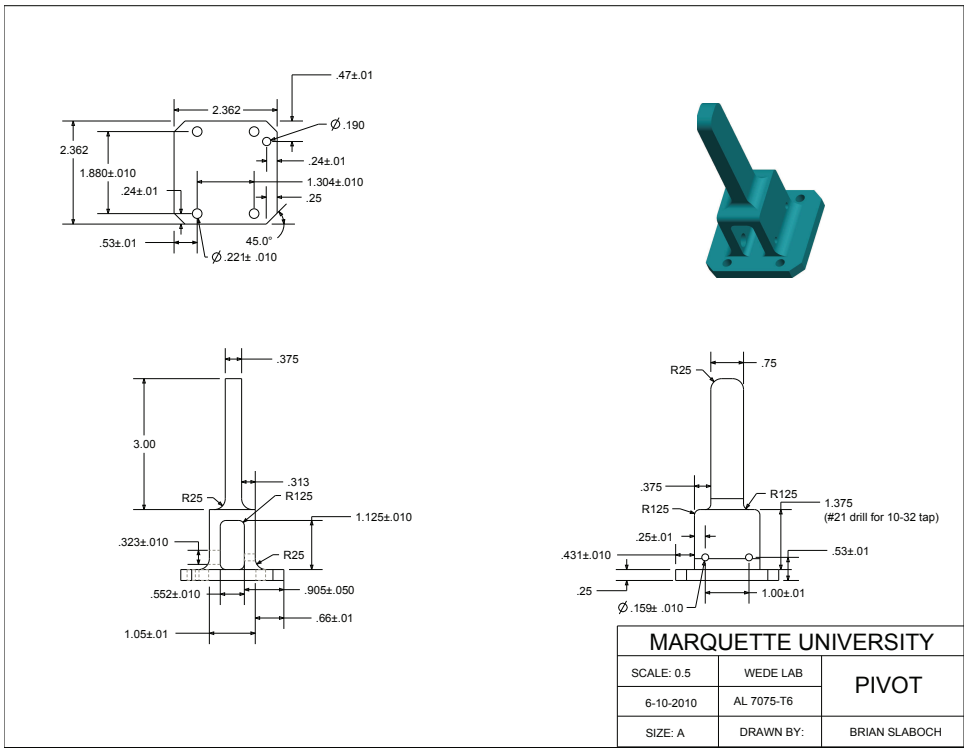

Figure 5.2: Detailed Drawing of the Pivot Arm

view of the base). This helps to simplify the kinematics because the positioning hinge is not offset from the attachment point of the robot. The last important feature is the 1 in. fillet that can be seen on the front view. This was necessary to ensure that the side of the base did not bend significantly during normal operation.

Figure 5.4 shows the final CAD model. This assembly was used to ensure that all of the parts could be assembled correctly. A motion simulation was created to ensure proper functionality. In addition, the part files were used to create a rapid prototype. This will be explained in further detail in the next section.

5.4 Prototype Testing

The physical prototype is shown in Fig. 5.5. It consists of a base, the pivot arm, and a rapid prototype gripper. The rapid prototype is made using a Z310 prototyping machine. The prototyping machine uses powder to create a solid 3D model. A plastic gripper was made to ensure that the real gripper would not be damaged during testing. The physical prototype was useful for several reasons.

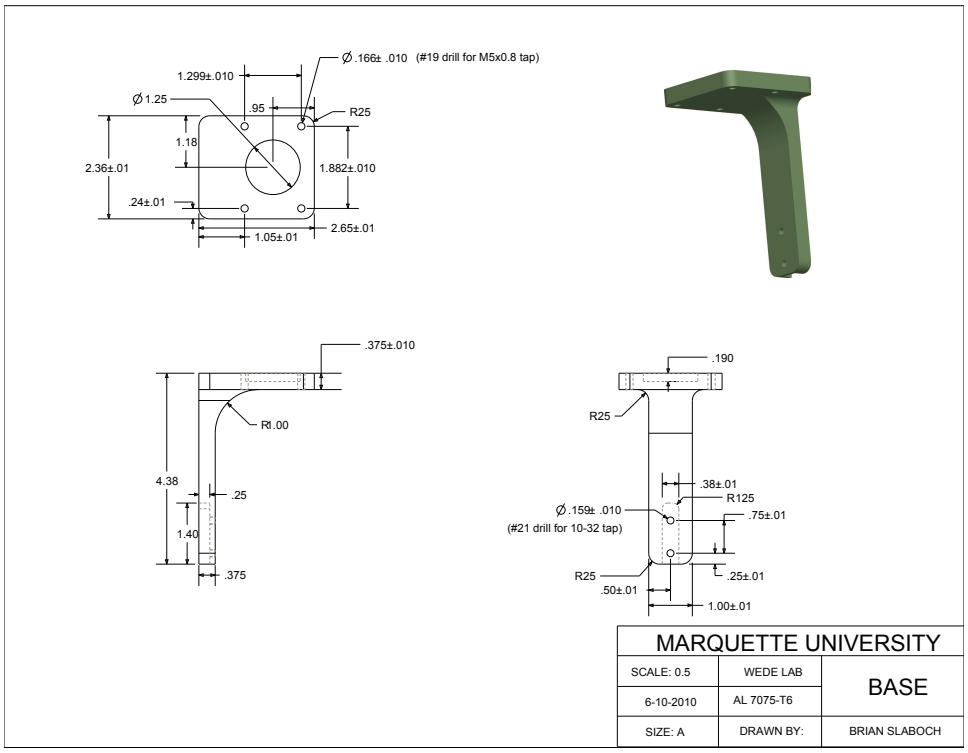

Figure 5.3: Detailed Drawing of the Base

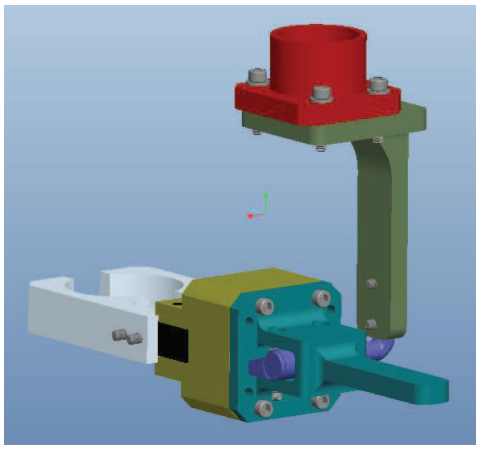

Figure 5.4: CAD Model

Having a physical prototype ensured that the parts could be assembled properly. In addition, it provided a reality check on the size of the components. After examining the prototype it was determined that the fillets could have a larger radius to reduce stress.

Ideally, this device would be tested on a SCARA type robot. However, the only available robot for testing was a Mistsubishi Melfa RV-3S six-axis robot. To

mimic the motion of a SCARA type robot the six DOF Mitsubishi robot was constrained to move with only four DOF.

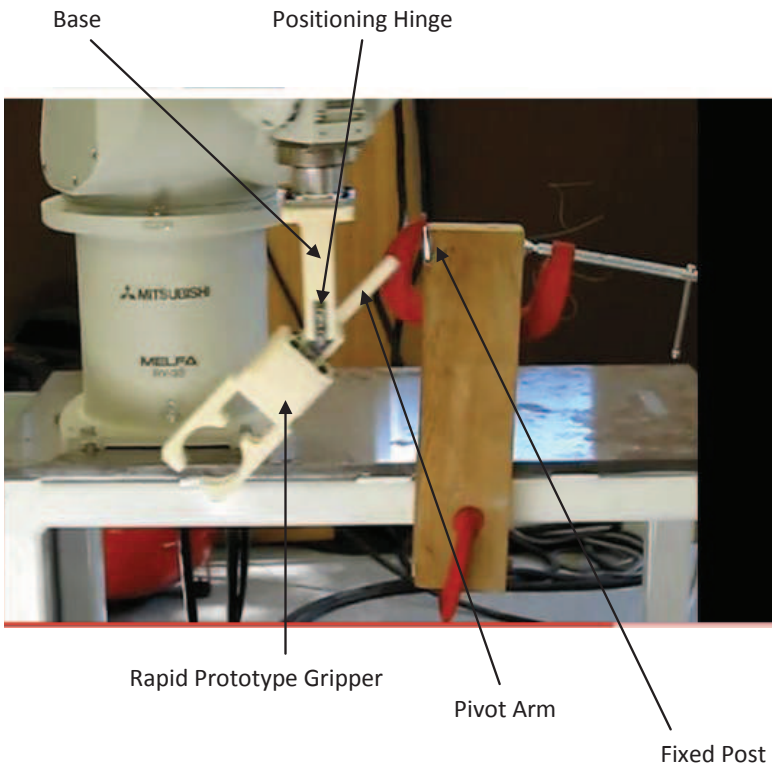

Figure 5.5: Rapid Prototype

5.4.1 Rapid Prototype Test 1

The first test was a ninety degree turn test shown in Fig. 5.6. This test is meant to mimic common pick and place assembly operations. For this test the pivot arm was placed next to the fixed post as shown in Fig. 5.6a. The 45° path algorithm was used to pivot the gripper 90° as shown in Fig. 5.6b. The speed on the robot was set to 30% of its maximum value.

The results of this test were encouraging. The gripper was successfully cycled through this process fifty times. Visual results showed that the gripper was routinely pivoted to approximately the same place after each cycle was completed.

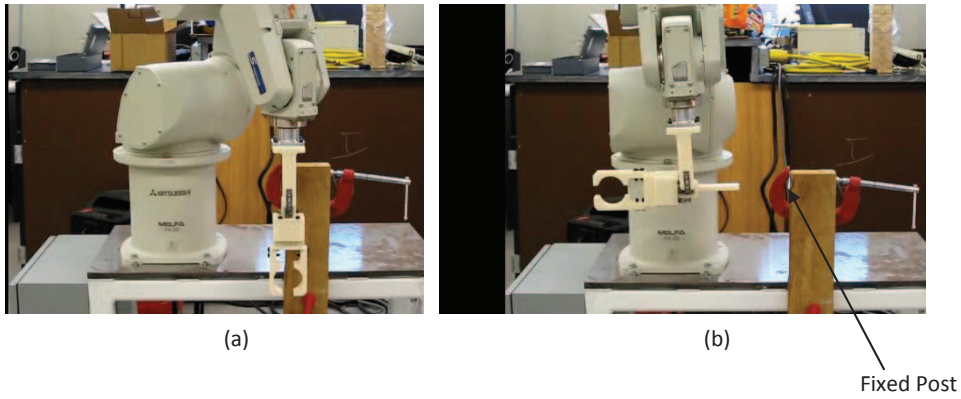

Figure 5.6: Test 1 with Rapid Prototype

5.4.2 Rapid Prototype Test 2

The second test performed was completed to determine the relative accuracy of the device. The end-effector was used to place a knife in an out of an angled knife holder. This is shown in Fig. 5.7. The robot was set at 10% of it maximum speed. The horizontal path algorithm was used to rotate the knife to the same angle as the slot in the knife holder. The knife was then placed into the knife holder. The knife was then pulled out of the knife holder, and the gripper was returned to its initial position. This cycle was repeated 25 times. This shows that the device is repeatable. The knife has a thickness of 1.2 mm and the slot it was placed into has a thickness of 4.42 mm. Thus, the prototype had a positioning error of ± 1.61 mm for this particular test.

After the program was run at 10% of the robot maximum speed, the speed was increased to 20%. Increasing the speed of the robot to 20% did not effect the results. The knife was still accurately placed in and out of the knife holder. However, this was not the case when the speed of the robot was further increased to 30%. At this higher speed the impact forces caused the pivot arm to rotate slightly more than desired. This means that the knife was not able to be correctly placed into the knife holder. As the knife approached the slot the tip of the knife blade caught onto the solid part of the knife holder.

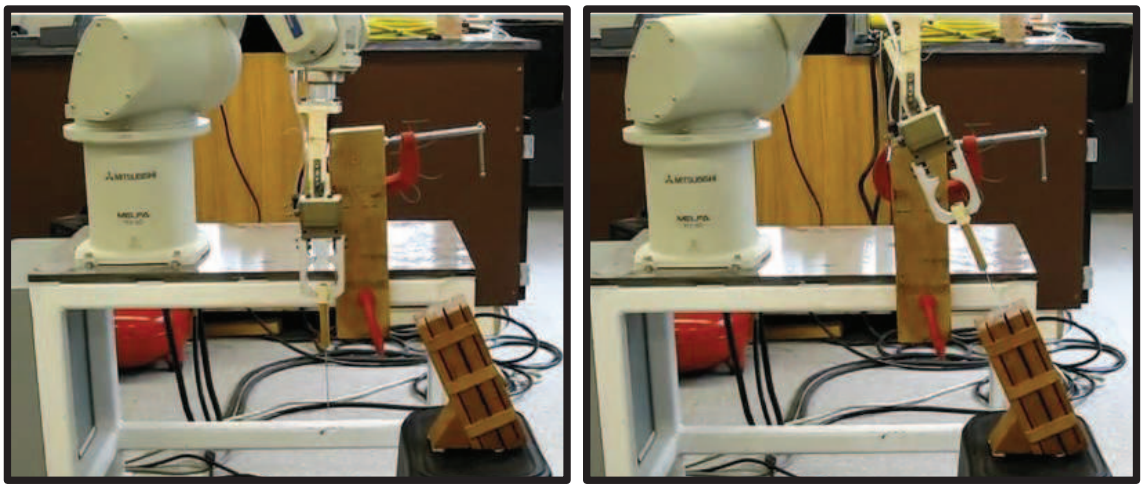

(a) (b)

Figure 5.7: Test 2 with Rapid Prototype

5.4.3 Design Modifications

From these tests multiple lessons were learned. The first lesson learned was that the fixed post was not sturdy enough. In these tests a hollow metal tube was clamped to a wood board. When the pivoting part was pressed through the fixed post, the post had a small vibration. A studier fixed post was used for the final design.

In Test 2 an important lesson was that the impact forces are high enough that at different robot speeds the gripper will be rotated a different amount. This relates back to the path planning algorithms developed in Chapter 3. As stated previously, these algorithms are developed based solely on the kinematics and not on the dynamics of the motion. In practice, the dynamics cannot be ignored. At very low speeds the impact forces can essentially be ignored. Therefore, it is recommended that the path planning algorithms be used at lower speeds. However, as will be seen in future sections, it is still possible to effectively use this device at higher speeds.

5.5 Final Design

The final product is shown in Fig. 5.8. Multiple tests were performed to determine the effectiveness of the design. This device was designed to be attached

to a Schunk PWG-60s angular two finger binary gripper. Figure 5.9 shows the gripper attached to the end-effector.

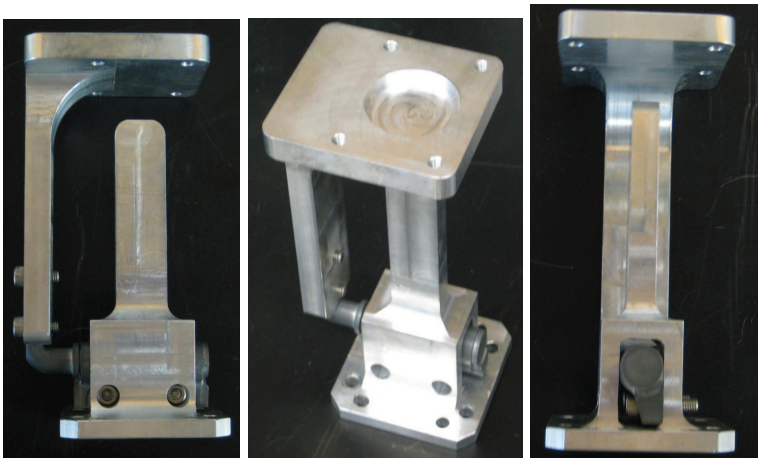

Figure 5.8: Final Design

5.5.1 Final Design Test 1

Figure 5.10 shows the setup for Test 1[2]. In this demonstration a block is picked up from the base plate of the robot, rotated to coincide with the angle of the ramp, and finally the block is placed on the ramp and it slides back down to the base plate of the robot. This cycle is then repeated multiple times. The robot speed was set to the 40% of the maximum value. During this test it was seen that the block was continuously brought to the correct angle, and there was almost no discrepancy between cycles.

5.5.2 Final Design Test 2

Figure 5.11 shows a 90° turn test that was performed. This is similar to the test that was performed with the prototype gripper. The difference was that the speed was set to the maximum allowable speed of the robot to prove that this device would work at high speeds. The device was put through approximately 200 cycles. The average cycle time was 1.8 s. This fell within the specified engineering requirements.

[2]This demonstration was completed with help from Kevin Flynn.

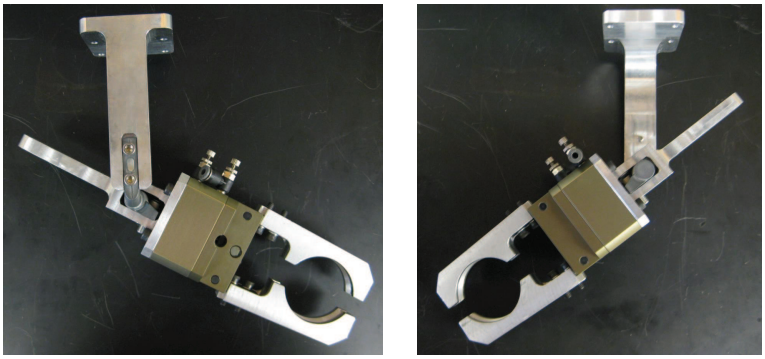

Figure 5.9: Final Design with Gripper

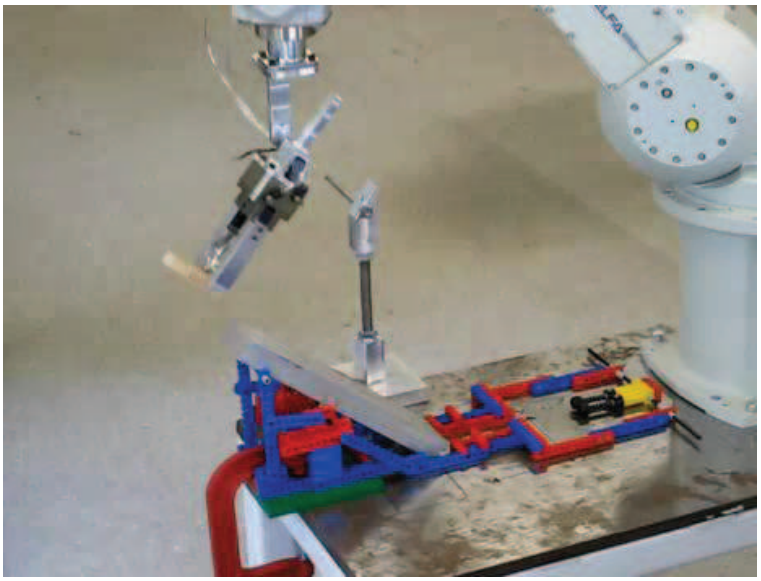

Figure 5.10: Final Design Test 1

5.5.3 Discussion

There were multiple lessons learned during the testing of the end-effector. As stated previously, a sturdier fixed post was needed. Fig. 5.10 shows the modified version of the fixed post. The new version includes a solid rod that is bolted to a stand that is clamped to the table of the robot. It was found that with this newly designed fixed post, there was less vibration upon impact. For laboratory testing the fixed post is simply clamped onto the stationary base plate of the robot. One reason for this is that it allows for the capability to move the fixed post to any location along the base plate. In practice, however, it is recommended that the fixed post be mounted directly to the base plate of the robot without using any clamps.

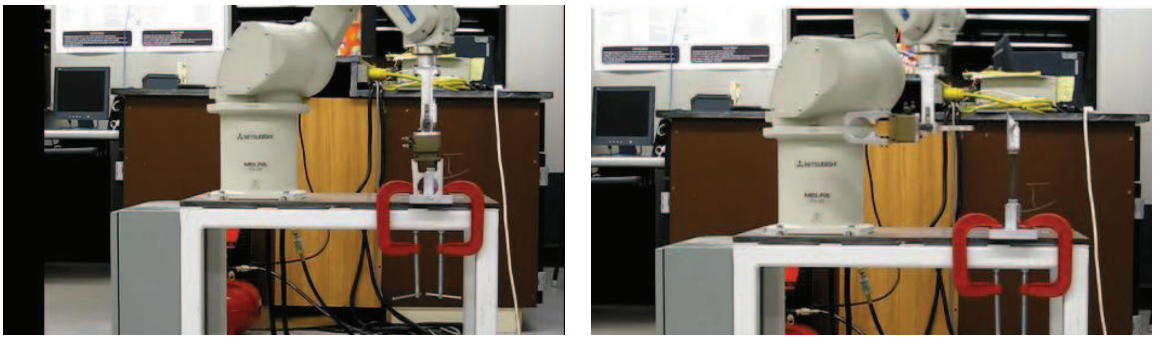

(a) (b)

Figure 5.11: Final Design Test 2

This will allow for a sturdier and more accurate system.

All of the tests were run using the teach-repeat option for the robot. One drawback that occurred in the 90° turn test (max speed case) was that the robot had to be programmed at its max speed. The program could not be created at a lower speed and then be modified to run at the max speed. The reason for this, as mentioned previously, was that due to the high impact forces the pivot arm would overshoot it desired angle. This meant that the programmer had to correct for this offset. The offset was significant enough that simply using the kinematic path planning from Chapter 3 would not produce the desired result.

The positive result from this was that it was relatively easy to program the robot to move the gripper to the desired angle. The kinematic path planning algorithms allowed one to determine approximately where the end-effector should be moved to. From there it was simple to correct for any additional springback from the high impact forces. Ideally, the motion planning algorithm will incorporate the dynamics. This will be an area of future work.

In this chapter material selection, positioning hinge selection, detail design, and experimental testing was discussed. The results from the experimental tests show that this gripper is industrially feasible, and it did meet the design requirements. The final product is a low weight gripper that provides a high torque to weight ratio.

CHAPTER 6

Contribution and Future Work

Orienting parts properly for robotic assembly applications is a difficult problem. Researchers have developed ways to orient parts ranging from parts feeders to complex anthropomorphic hands. Each of these solutions works well for specific types of robotic assembly applications. This thesis focused on a particular subset of robotic assembly tasks. The goal of this research was to develop an end-effector that could be used in an industrial setting to provide a selectable DOF to a SCARA type robot. The next section outlines the specific contributions of this research.

6.1 Contributions of this Research

The contributions of this research are as follows:

- A novel end-effector was designed, built, and tested.
- The flexibility in this design is a key contribution. Many grippers that are aimed at providing an added DOF only work for polyhedral parts. This design is built to work with any custom gripper that can pick up a wider range of parts.
- New path planning techniques were developed to be used with the end-effector. Most path planning techniques are aimed at collision avoidance. This is an application in which obstacles can be used as an advantage.
- This end-effector shows how the built in controls of a robot can be used to aid in part manipulation. The end-effector can be designed as part of the overall system as opposed to a separate entity.
- A dynamic analysis was completed to determine the required resistance torque for the positioning hinge. The closed form solution allows for designers to

easily specify an appropriate positioning hinge for a particular application.

It is to be emphasized that part of the beauty in this design is in its simplicity. A simple mechanical device can be used to replace a complex electrical or pneumatic rotary actuator. This end-effector is not a panacea for all robotic assembly applications. However, this is a step in the right direction. The next section will explore future research opportunities based on this work.

6.2 Future Work

There is a considerable amount of future work that can be done based on this research. There are many questions that need to be answered before this work can be implemented in an industrial setting.

6.2.1 Dynamic Analysis

In this thesis a dynamic analysis was completed that enables a designer to determine the necessary torque the positioning hinge must provide to ensure the positioning hinge does not move due to either inertial forces or gravity. However, there is more dynamic analysis that needs to be completed. Most importantly, there are significant impact forces that occur when the pivot arm makes contact with the fixed post at high speeds. If the impact forces are too high the positioning hinge will rotate more than the desired angle of rotation determined from the kinematic modeling. Therefore, impact forces should be reduced as much as possible. One way to reduce impact forces would be to coat the fixed post with rubber to help absorb impact forces. Also, the robot's end-effector may be moved at a slow enough speed that impact forces can be ignored.

The impact forces could be used to determine the desired angle of rotation. This could be determined experimentally. For horizontal path motion the angle of rotation, θ_f, could be a function of multiple variables as shown in Eq. 6.1.

$$\theta_f = f(m_p, m_g, v_h, h, \tau), \tag{6.1}$$

where m_p and m_g are the mass of the part and the gripper, v_h is the horizontal velocity of the end-effector, h is the distance from the centerline of the positioning hinge to the center of the fixed post, and τ is the amount of torque provided by the positioning hinge. This model could be used in conjunction with the kinematic analysis in this thesis to create a more accurate system.

Another dynamic problem of interest is the amount of overshoot that may occur as the gripper is being rotated. The momentum from the gripper may cause overshoot. This can be determined by using a standard dynamic analysis.

6.2.2 Kinematic Analysis

This thesis outlined three related path planning algorithms that may be used to obtain the desired angle of rotation. In each of these path planning algorithms the following assumptions were made:

1. Only one fixed post was used.
2. The fixed post was cylindrical.
3. The pivot arm was a flat surface.

With these assumptions in place three path planning algorithms were developed. Each of the path planning algorithms involved moving the end-effector in a straight line, and the algorithms are all related in a general way. Only straight line paths were considered because moving the end-effector in a straight line reduced the cycle time.

However, there are still kinematic questions that need to be answered. A more comprehensive way to approach the kinematic problem would be to approach the problem from a complete system perspective. The goal of the kinematic problem is the complete the following steps in the most efficient and accurate way possible:

1. Grasp the part.
2. Rotate the gripper from its initial angle to a desired angle.
3. Assemble the part.

4. Rotate the gripper back to its initial angle.

5. Repeat this process.

When viewing this problem from a system perspective the problem becomes more complex. There are new questions that would need to be answered. For instance, where should the fixed post be placed in the robot's workspace to provide optimal performance? Additionally, there may be advantages to using more than one fixed post. By strategically placing fixed post's in the robot's workspace an optimal solution could be obtained.

Another consideration that would need to be taken into account is the design of both the fixed post and the pivot arm. The kinematic equations developed in this thesis were dependent on the radius, r, of the fixed post. Thus, the design of both the fixed post and the pivot arm critical in the path planning.

6.2.3 Stress Analysis

A standard stress analysis could be completed on the fixed post to ensure that it can withstand the continuous impact forces that occur. Additionally, a standard stress analysis could be completed on the pivot arm to ensure that it does not yield to the continuous impact forces.

6.2.4 Robustness

The most important part of a robotic system is robustness. In this design a positioning hinge was used that will work for 20,000 cycles. More research needs to be completed to determine a way to create more robust positioning hinges that will last for longer periods of time. Additionally, over time there may be wear on both the pivot arm and the fixed post. Research needs to be done to determine how much of an impact wear will have on the overall system.

REFERENCES

[1] M.T. Zhang and K. Goldberg. Gripper point contacts for part alignment. *IEEE Transactions on Robotics and Automation*, 18(6):902–910, December 2002.

[2] S. Jacobsen, J. Wood, K. Bigger, and E. Iverson. The Utah/MIT hand: Work in progress. *International Journal of Robotics Research*, 4(3):21–50, 1984.

[3] B. Carlisle, K. Goldberg, A. Rao, and J. Wiegley. A pivoting gripper for feeding industrial parts. In *Proceedings of the 1994 IEEE International Conference on Robotics and Automation*, volume 2, pages 1650–1655, San Diego, CA, May 1994.

[4] A. Rao, D.J. Kriegman, and K. Goldberg. Complete algorithms for feeding polyhedral parts using pivot grasps. In *IEEE Transactions on Robotics and Automation*, volume 12, pages 331–342, April 1996.

[5] G. Boothroyd, C. Poli, and L.E. Murch. *Automatic Assembly*. Marcel Dekker, Inc., New York, 1982.

[6] G. Boothroyd, P. Dewhurst, and W. Knight. *Product Design for Manufacture and Assembly*. Marcel Dekker, Inc., New York, 1994.

[7] M. A. Peshkin and A.C. Sanderson. Planning robotic manipulation strategies for workpieces that slide. *IEEE Transactions on Robotics and Automation*, 4(5):696–700, October 1988.

[8] M.T. Zhang, K. Goldberg, G. Smith, R.-P. Berretty, and M. Overmars. Pin design for part feeding. *Robotica*, 19(6):695–702, November/December 2001.

[9] G. Causey and R. Quinn. Design of a flexible part feeding system. In *Proceedings of IEEE International Conference on Robotics and Automation*, Albuquerque, NM, 1997.

[10] M.T. Mason and J.K. Salisbury. *Robot Hands and the Mechanics of Manipulation*. MIT Press, Cambridge, MA, 1985.

[11] William T. Townsend. The BarrettHand grasper programmably flexible part handling and assembly. *Industrial Robot: An International Journal*, 27(3):181–188, 2000.

[12] Jiansheng Dai and Zhang Qixian. Metamorphic mechanisms and their configuration models. *Chinese Journal of Mechanical Engineering*, 13(3):212–218, 2000.

[13] Jacob A. Ziesmer and Philip A. Voglewede. Design, analysis and testing of a metamorphic gripper. In *Proceedings of the ASME 2009 International DETC*, 2009. DETC2009-87512.

[14] K.M. Lynch and M.T. Mason. Dynamic manipulation with a one joint robot. In *Proceedings of the 1997 IEEE International Conference on Robotics and Automation*, pages 359–366, Albuquerque, NM, April 1997.

[15] K.M. Lynch, N. Shiroma, H. Arai, and K. Tanie. Collision-free trajectory planning for a 3-dof robot with a passive joint. *The International Journal of Robotics Research*, 19(12):1171–1184, December 2000.

[16] R. Eggert, editor. *Engineering Design*. Pearson Prentice Hall, Upper Saddle River, NJ, 1999.

[17] J. Latombe. *Robot Motion Planning*. Kluwer Academic Publishers, sixth edition, 2001.

[18] J. Ginsberg. *Mechanical and Structural Vibrations: Theory and Applications*. John Wiley and Sons, 2001.

APPENDIX A

The derivation below is for the distance, d, from (x_i, y_i) in terms of h, R, and θ_f as shown in Fig. A.1

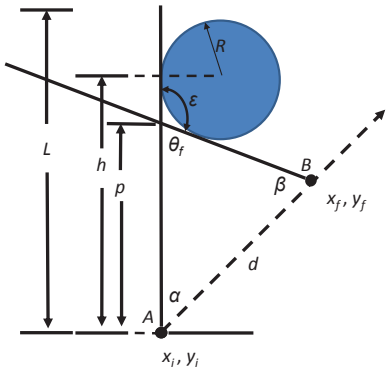

Figure A.1: 45° Angle Schematic

From Fig. A.1

$$\epsilon = \pi - \theta_f \tag{A.1}$$

$$\beta = \pi - \alpha - \theta_f. \tag{A.2}$$

From Fig. A.2

$$R = l \sin \frac{\epsilon}{2}. \tag{A.3}$$

Substituting Eqn. A.1 into Eqn. A.3 gives

$$R = l \cos \frac{\theta_f}{2}. \tag{A.4}$$

The distance p can be written as

$$p = h - l \sin \frac{\pi - \epsilon}{2}, \tag{A.5}$$

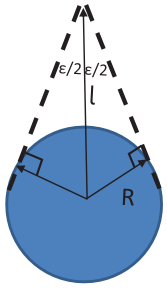

Figure A.2: Relation Between ϵ and l

which can be simplified to

$$p = h - l \sin \frac{\theta_f}{2}. \tag{A.6}$$

Substituting the relation between R and l from Eqn. A.4 gives

$$p = h - \frac{R \sin \frac{\theta_f}{2}}{\cos \frac{\theta_f}{2}}. \tag{A.7}$$

The law of sines states that

$$\frac{\sin \theta_f}{d} = \frac{\sin \beta}{p} \tag{A.8}$$

Substituting β and p into Eqn. A.8 and solving for d gives

$$d = \frac{\sin \theta_f}{\sin (\pi - \alpha - \theta_f)} \left(h - R \tan \frac{\theta_f}{2} \right). \tag{A.9}$$